Note: Yellow highlights are revisions based on first round of comments. Grey highlights are revisions based on second round of comments.

# Vertical profiles of light absorption and scattering associated with black-carbon particle fractions in the springtime Arctic above 79°N

W. Richard Leaitch[1], John K. Kodros[2], Megan D. Willis[3, a], Sarah Hanna[4], Hannes Schulz[5], Elisabeth Andrews[6,8], Heiko Bozem[7], Julia Burkart[3, b], Peter Hoor[7], Felicia Kolonjari[1], John A. Ogren[8], Sangeeta Sharma[1], Meng Si[4], Knut von Salzen[9], Allan K. Bertram[4], Andreas Herber[5], Jonathan P. D. Abbatt[3], Jeffrey R. Pierce[2]

[1] - Environment and Climate Change Canada, Toronto, ON, Canada
[2] – Department of Atmospheric Science, Colorado State University, Fort Collins, CO, USA
[3] – Department of Chemistry, University of Toronto, Toronto, ON, Canada
[a] – now: Lawrence Berkeley National Laboratory, Chemical Sciences Division, Berkeley, CA, USA
[b] - now: Aerosol Physics and Environmental Physics, University of Vienna, Austria
[4] – Department of Chemistry, University of British Columbia, Vancouver, BC, Canada
[5] – Alfred Wegener Institute, Helmholtz Center for POLAR and Marine Research, Bremerhaven, Germany
[6] - University of Colorado, Boulder, CO, USA
[7] – Institute of Atmospheric Physics, Johannes Gutenberg-University, Mainz, Germany
[8] - National Oceanic and Atmospheric Administration (NOAA), Boulder, CO, USA
[9] - Environment and Climate Change Canada, Victoria, BC, Canada

*Correspondence to:* W. Richard Leaitch (leaitchs@gmail.com); Jeffrey R. Pierce (jeffrey.pierce@colostate.edu)

**Abstract.** Despite the potential importance of black carbon (BC) to radiative forcing of the Arctic atmosphere, vertically-resolved measurements of the particle light scattering coefficient ($\sigma_{sp}$) and light absorption coefficient ($\sigma_{ap}$) in the springtime Arctic atmosphere are infrequent, especially measurements at latitudes at or above 80°N. Here, relationships among vertically-distributed aerosol optical properties ($\sigma_{ap}$, $\sigma_{sp}$, and single scattering albedo or SSA), particle microphysics and particle chemistry are examined for a region of the Canadian archipelago between 79.9°N and 83.4°N from near the surface to 500 hPa. Airborne data collected during April, 2015, are combined with ground-based observations from the observatory at Alert, Nunavut and simulations from the GEOS-Chem-TOMAS model (Kodros et al., 2018) to further our knowledge of the effects of BC on light absorption in the Arctic troposphere. The results are constrained for $\sigma_{sp}$ less than 15 $Mm^{-1}$, which represent 98% of the observed $\sigma_{sp}$, because the single scattering albedo (SSA) has a tendency to be lower at lower $\sigma_{sp}$, resulting in a larger relative contribution to Arctic warming. At 18.4 $m^2 g^{-1}$, the average BC mass absorption coefficient (MAC) from the combined airborne and Alert observations is substantially higher than the two averaged modelled MAC values (13.6 $m^2 g^{-1}$ and 9.1 $m^2 g^{-1}$) for two different internal mixing assumptions, the latter of which is based on previous observations. The higher observed MAC value may be explained by an underestimation of BC, the presence of small amounts of dust and/or possible differences in BC microphysics and morphologies between the observations and model. In comparing the observations and simulations, we present $\sigma_{ap}$ and SSA, as measured, and $\sigma_{ap}/2$ and the corresponding SSA to encompass the lower modelled MAC that is more consistent with accepted MAC values. Median values of the measured $\sigma_{ap}$, rBC and organic component of particles all increase by a factor of 1.8±0.1 going from near-surface to 750 hPa, and values higher than the surface persist to 600 hPa. Modelled BC, organics, and $\sigma_{ap}$ agree with the near-surface measurements, but do not reproduce the higher values observed between 900 hPa and 600 hPa. The differences between modelled and observed optical properties follow the same trend as the differences between the modelled and observed concentrations of the carbonaceous components (black and organic). Model-observation discrepancies may be mostly due to the modelled ejection of biomass burning particles only into the boundary layer at sources. For the assumption of the observed MAC value, the SSA range between 0.88 and 0.94, which is significantly lower than other recent estimates for the Arctic, in part reflecting the constraint of $\sigma_{sp}$ <15 $Mm^{-1}$. The large uncertainties in measuring optical properties and BC as well as the large differences between measured and modelled values, here and in the literature, argue for improved measurements of BC and light

absorption by BC as well as more vertical profiles of aerosol chemistry, microphysics, and other optical properties in the Arctic.

## 1 Introduction

Aerosol particles responsible for Arctic haze (Mitchell, 1956) originate from mid-latitude pollution sources during winter and spring (e.g. Holmgren et al., 1974; Rahn et al., 1977; Rahn, 1981; Shaw, 1983; Barrie and Hoff, 1985; Radke et al., 1984; Schnell and Raatz, 1984; Barrie, 1986). During late spring and summer, the Arctic is cleansed of haze particles by increased levels of precipitation (e.g. Garrett et al., 2011) resulting in a much cleaner, sometimes pristine, troposphere. At lower altitudes, Europe and Northern Asia are thought to be the dominant source regions of Arctic haze with contributions from south/central Asian sources dominating at higher altitudes (e.g. Stohl, 2006; Fisher et al., 2011; Sharma et al., 2013; Qi et al., 2017; Xu et al., 2017). Although surface-based concentrations of Arctic haze components have declined since studies of Arctic haze first began (Heidam et al., 1999; Sirois and Barrie, 1999; Sharma et al., 2004; 2006; Quinn et al., 2009; Hirdman et al., 2010; Sinha et al., 2017), it is unclear how total atmospheric burdens have changed (e.g. Sharma et al., 2013) and horizontal inhomogeneities with scales of 50-100 km (Hansen and Rosen, 1985) complicate this issue.

Radiative forcing by Arctic haze particles may be an important regional driver of Arctic climate change (e.g. Law and Stohl, 2007; Quinn et al., 2008). Characterized by a unimodal number distribution centered between 200 and 300 nm diameter (e.g. Bigg, 1980; Heintzenberg, 1980; Radke et al., 1984; Leaitch et al., 1989; Staebler, 1994), the effectiveness of Arctic haze particles at scattering light (e.g. Delene and Ogren, 2002; Schmeisser et al., 2017) is one reason why the net effect of the Arctic aerosol has been estimated to cool the Arctic atmosphere (Najafi et al., 2015; Navarro et al., 2016). Black carbon (BC) is the primary anthropogenic light-absorbing component of Arctic haze, (e.g. Leighton, 1983; Valero et al., 1984; Hansen and Rosen, 1984; Blanchet and List, 1987; Valero et al., 1989; Pueschel and Kinne, 1995; Hansen and Nazarenko, 2004; Flanner et al., 2007; McConnell et al., 2007; Law and Stohl, 2007; Quinn et al., 2008; Schindell and Faluvegi, 2009; Brock et al., 2011). Mitigation of BC emissions has been proposed as a provisional means of slowing Arctic warming (Shindell and Faluvegi, 2008; Kopp and Mauzerall, 2010; Stohl et al., 2015; Sand et al., 2016), but considerable uncertainty surrounds radiative forcing by BC in the Arctic. Despite profiles of black carbon and optical properties in recent years (e.g. Brock et al., 2011; McNaughton et al., 2011; Schwarz et al., 2010; Spackman et al., 2010; Wofsy et al., 2011; Ferrero et al., 2016; Markowicz et al., 2017) there remains a shortage of such

observational data that limits evaluation of models of Arctic BC and light absorption (e.g. Samset et al., 2013), because the Arctic is subject to transport from many pollution sources at southern latitudes during winter and spring, and variability exists with altitude, with location and from year-to-year.

Here, we use a combination of airborne and ground-based observations plus modelling to examine particle light scattering coefficients ($\sigma_{sp}$), light absorption coefficients ($\sigma_{ap}$), and single scatter albedos (SSA) at the green wavelength of 550 nm from near the surface to 500 hPa over a region of the Arctic Ocean between 79.9°N and 83.4°N. Recent Arctic studies, ground-based and airborne, indicate SSA values ranging from 0.92 to 0.97 during the month of April for a wavelength of 550 nm (Delene and Ogren, 2002; Brock et al., 2011; McNaughton et al., 2011; Schmeisser et al., 2017), or roughly 5% of the light incident on a population of Arctic haze particles is absorbed. The present work, part of the Canadian Network on Climate and Aerosols: Addressing Key Uncertainties in Remote Canadian Environments or NETCARE, contributes knowledge concerning Arctic optical properties and warming of the Arctic lower troposphere by BC during April at higher latitudes.

Airborne measurements of $\sigma_{ap}$ that are based on transmission of light through a filter, as used here, are constrained by instabilities during changes in pressure (i.e. altitude) and generally higher detection limits (DL) associated with flight conditions. To reduce the skewness of observations imposed by these constraints, we expand our dataset of $\sigma_{ap}$ values by employing a linear relationship between measured $\sigma_{ap}$ and the refractory black carbon mass concentrations (rBC) of Schulz et al. (2018). This approach enables a more comprehensive representation of values below DL. In the airborne component of this dataset, over 98% of one-minute averages of $\sigma_{sp}$ exceeding detection limit (0.9 $Mm^{-1}$) are below 15 $Mm^{-1}$. By constraining the discussion to values of $\sigma_{sp}$ less than 15 $Mm^{-1}$, we address the largest component of Arctic haze exclusive of the direct influence from strong plumes. Since most Arctic pollution in April is from long-range transport, the lower $\sigma_{sp}$ suggests that these particles on average spent longer times in the Arctic atmosphere and thus are more indicative of the "chronic" Arctic haze discussed by Brock et al. (2011). Further, the SSA for particle populations that fall within this constraint have been found to decrease more sharply with decreasing $\sigma_{sp}$ (e.g. Targino et al., 2005; Andrews et al., 2011), making these populations more efficient at warming of the atmosphere. Our primary objective is to demonstrate the large uncertainty in our knowledge of the absorption by BC at lower $\sigma_{sp}$ in an area of the high Arctic with a low frequency of observations. Details of the methods employed are

described in Section 2. In Section 3, results are presented and vertical profiles of $\sigma_{ap}$ and SSA are compared with simulated values. Section 4 is a broader discussion of the results, and conclusions are given in Section 5.

## 2 Methods

### 2.1 Observations overview

Ten research flights were conducted in the Arctic using the Alfred Wegener Institute (AWI) POLAR 6 aircraft beginning on April 5, 2015 and ending on April 21, 2015. The first and only flight from Longyearbyen, Svalbard, Norway is not discussed here as it dealt with some instrument and sampling issues. Subsequently, four flights were conducted from Alert, Nunavut, Canada during April 7-9 (two flights on April 8), two flights from Eureka, Nunavut, Canada (April 11 and 13) and three flights from Inuvik, Northwest Territories, Canada on April 20-21 (two flights on April 20). Tracks of the flights out of Alert and Eureka can be found in Kodros et al. (2018), Schulz et al. (2018) and Willis et al. (2018). The flights out of Inuvik were conducted within a 300 km radius of Inuvik (68.4°N; 133.7°W). Sampling of submicron particles from the POLAR 6 during NETCARE is discussed by Leaitch et al. (2016), Schulz et al. (2018) and Willis et al. (2018). All airborne and model data presented here are referenced to a temperature of 20°C and pressure of 1013.25 hPa. The POLAR 6 data are restricted to between 2 minutes after takeoff and 2 minutes prior to landing to avoid local contamination.

Ground-based observations of $\sigma_{sp}$, $\sigma_{ap}$, rBC and particle microphysics are routinely conducted at the Dr. Neil Trivett Global Atmospheric Watch Observatory at Alert, Nunavut (82.5°N, 62.5°W). The site is approximately 7 km south-east of the main Alert station that is operated by the Canadian Department of National Defense. The impact of the camp on observations at the Alert Observatory (hereafter, referred to as Alert) has been found to be insignificant for particles larger than about 50 nm diameter (Leaitch et al., 2018), and the observations are filtered for air arriving from within a 45° arc centred on the station. The Alert optical properties data reported here are for particles less than 1 μm diameter.

### 2.2 Aerosol optical measurements

Particle light scattering coefficients ($\sigma_{sp}$) at wavelengths of 450 nm, 550 nm and 700 nm were measured with a TSI Model 3563 three-wavelength volume integrating nephelometer on the POLAR 6 and at Alert. To account for the absence of a forward scattering measurement where the collimated light beam is dumped (i.e., truncation of the total scattering between 0-7° and 170-180°), the correction described by Anderson and Ogren

(1998) was applied. A span check of the nephelometer calibration is routinely performed at Alert using $CO_2$, and span checks of the nephelometer used on the POLAR 6 were conducted before and after the study.

Values of $\sigma_{ap}$ at Alert are derived from a three-wavelength Particle Soot Absorption Photometer (PSAP), as discussed by Sharma et al. (2017). The $\sigma_{ap}$ on the POLAR 6 were measured using a Continuous Light Absorption Photometer (CLAP), a three-wavelength filter-based instrument operating at 467 nm, 528 nm and 652 nm. Based on the PSAP design, the CLAP, designed and built by NOAA, samples consecutively on one of eight spots on one 47 mm glass-fibre filter (Pallflex type E70-2075W), which improves functionality in situations where filter changes are more difficult, such as remote sites and aircraft (Ogren et al., 2017). For both the PSAP and CLAP, the $\sigma_{ap}$ are derived from the change in light transmission through a spot on the filter accumulating particles relative to light transmission through a reference spot. Both the PSAP and CLAP data were corrected for multiple scattering arising from the filter medium and accumulating particles using an empirical algorithm described by Bond et al. (1999) and Ogren (2010). To avoid artifacts associated with filter disturbances due to rapid pressure fluctuations, the POLAR 6 absorption data are limited to in-flight pressure variations, as recorded within the nephelometer, of less than 2 hPa over a two-minute period encompassing each one-minute sample. Recently, Düsing et al. (2019) found that changes in water uptake by filter material used in particle absorption measurements can influence the light absorption measurement. In the present case, because the ambient temperatures were -20°C or colder and the temperatures at the intake of the nephelometer, which was situated next to the CLAP, ranged from +14°C to +30°C, we expect little influence of relative humidity on our results. As discussed in Section 3.2, in some circumstances these corrections may fail to correct overestimates of $\sigma_{ap}$ due to multiple scattering (Cappa et al., 2008a; 2008b; Lack et al., 2008; Sinha et al., 2017).

The estimated detection limits (DL) for $\sigma_{ap}$ and $\sigma_{sp}$ on the POLAR 6 are 0.75 $Mm^{-1}$ and 0.9 $Mm^{-1}$, respectively, at 550 nm wavelength and for one-minute averages. The DL are calculated from the maximum of two times the standard deviation of the raw measurement during in-flight zeroes, which are also constrained to pressure variations of 2 hPa or less. The $\sigma_{sp}$ DL was adjusted for the truncation correction, and the $\sigma_{ap}$ DL was adjusted for multiple scattering. Of approximately 2000 one-minute averaged data points, collected over nine flights, 220 absorption data points remain after scrutiny for DL and pressure variations. Uncertainties in the POLAR 6 $\sigma_{ap}$ are considered in Section 3.3.

The DLs for $\sigma_{ap}$ and $\sigma_{sp}$ measured at Alert are 0.1 $Mm^{-1}$ for and 0.4 $Mm^{-1}$, respectively, and represent DLs for the one-hour averages of Alert data used here. Based on Sherman et al. (2015) and Ogren et al. (2017),

uncertainties in $\sigma_{ap}$ at 1 $Mm^{-1}$ and $\sigma_{sp}$ at 10 $Mm^{-1}$ are 60% and 24% respectively. After discriminating for local influences and removal of compromised data (e.g. zeroes), the Alert data set comprises 1505 one-hour averages, or approximately 70% of the February-April, 2015 time period. The months of February and March are included to broaden the comparison with the model results.

The $\sigma_{ap}$ from the POLAR 6 and from Alert were adjusted to the nephelometer wavelengths assuming a $1/\lambda$ relationship, and the $\sigma_{ap}$, $\sigma_{sp}$ and SSA for both platforms are reported for wavelengths of 450 nm (blue), 550 nm (green) and 700 nm (red). The SSA, given by $\sigma_{sp}/(\sigma_{sp}+\sigma_{ap})$, were calculated for the green values of $\sigma_{sp}$ and $\sigma_{ap}$.

**2.3 rBC and Physical Measurements**

Size distributions for particles with diameters in the range of 85 - 1000 nm were measured on the POLAR 6 using an Ultra High Sensitivity Aerosol Spectrometer (UHSAS, Droplet Measurement Technology Inc); hereafter, all particle sizes are given as diameters. The UHSAS is a laser-based aerosol spectrometer. Checks of concentration and sizing were done with nearly monodisperse particles of ammonium sulphate. Details of the measurements used here are discussed by Schulz et al. (2018). The size distributions from the UHSAS are used to estimate submicron particle volume concentrations. Submicron particle volume concentrations at Alert are estimated from size distribution measurements with a TSI 3034 SMPS, previously discussed by Leaitch et al. (2013; 2018). As discussed by Willis et al. (2018), size distributions from the UHSAS were compared with those from the TSI 3034 SMPS at the Alert from four flights when the POLAR 6 flew between 60 m and 200 m above the ocean (sea ice) surface a few kilometres north of Alert. The volume concentrations calculated from the two measurements for the 85-500 nm size range compared within 20% for all flights.

Refractory black carbon (rBC) was measured on the POLAR 6 using a Droplet Measurement Technologies Inc. Single Particle Soot Photometer (SP2). The SP2 detects individual particles using an intra-cavity Nd:YAG laser operating at 1064 nm. Incandescence from components of particles absorbing at 1064 nm (i.e. BC) is detected by a pair of photomultiplier tubes, and the peak amplitude of the thermal radiation is proportional to the mass of refractory material (Moteki and Kondo, 2007; Slowik et al., 2007). The detection range of the SP2 used here is 0.60 fg rBC to 330 fg rBC, or approximately 85-700 nm mass equivalent diameter for a rBC density of 1.8 g $cm^{-3}$ (Bond and Bergstrom, 2006; Bond et al., 2013). Mass calibrations are based on Fullerene soot particles that were size selected using a differential mobility analyser. The mobility diameters

were converted to rBC mass concentrations following Gysel et al. (2011). Schulz et al. (2018) describe the dataset used here, and they estimate the uncertainty at ±15%. The rBC measurements conducted at Alert, also made using a SP2, are discussed by Sharma et al. (2017).

Non-refractory aerosol mass concentrations were measured aboard POLAR 6 with an Aerodyne High Resolution Time-of-Flight Aerosol Mass Spectrometer (ToF-AMS) (DeCarlo et al., 2006). These measurements are described in detail by Willis et al. (2019). Briefly, the ToF-AMS measured non-refractory aerosol between about 70 – 700 nm vacuum aerodynamic diameter. Detection limits for sulfate and total organic aerosol, based on 10 s time resolution, were 0.01 μg/m3 and 0.08 μg/m3, respectively.

Coarse particles (>2 μm diameter) on the POLAR 6 were measured with a GRIMM Model 1.129 Optical Particle Counter. Model 1.129 measures particles larger than 0.25 μm, but only the coarse particle concentrations are used here. As shown by comparisons with a Particle Measuring Systems FSSP-300 probe operated under one wing of the POLAR 6, the coarse particles tend to be sampled less effectively than the submicron particles, but they are still an indicator of the presence of coarse particles, and, more importantly, the coarse particles entering the POLAR 6 sample manifold.

**2.4 Modelling**

The observations of $\sigma_{sp}$, $\sigma_{ap}$ and SSA are compared to version 10.01 of the GEOS-Chem chemical-transport model (geos-chem.com), driven by MERRA re-analysis meteorology fields. The February-April 2015 simulation was preceded by a 2-month spin-up. This version of GEOS-Chem uses a horizontal resolution of 4 degrees latitude by 5 degrees longitude (approximately 440 km x 72 km in the flight region near Alert and Eureka, and 440 km x 200 km near Inuvik) with 47 vertical layers. Relevant to the observations presented here, 24 vertical layers cover the pressure region from the surface to 500 hPa, 12 of which are from the surface to 850 hPa spaced equally by 15.5 hPa. Aerosol microphysics is simulated using TwO Moment Aerosol Sectional (TOMAS) microphysics scheme (Adams and Seinfeld, 2002) coupled with GEOS-Chem (known as "GEOS-Chem-TOMAS"), including tracers for sulfate, BC, organic aerosol, sea salt, dust, and aerosol water. More details are found in Adams and Seinfeld (2002), Lee et al. (2013), Lee and Adams (2012), and Kodros et al. (2018). Here, particle water is excluded from the calculations because the observed particles were relatively dry: during the flights, the outside air temperature was -15°C or less and the measured temperature of air entering the nephelometer, which was situated near the CLAP, ranged between +14°C or greater, indicating very low values of relative humidity at the point of measurement; also, no significant particle water was indicated in the ToF-AMS data.

Aerosol optical properties are calculated using monthly averaged aerosol mass and number concentrations with refractive indices from the Global Aerosol Dataset (GADS; Kopke et al., 1997). To calculate aerosol optical properties, we assume two of the BC mixing states discussed by Kodros et al. (2018): 1) "Allcore", in which BC is fully mixed with other chemical species in a core-shell morphology within each size section, where BC forms the core of the particle and hydrophilic aerosol species form a concentric shell around the BC core; 2) "Rshell", in which BC is mixed within a particle, again as a core surrounded by hydrophilic species, but the size-dependent fraction of BC–containing particles core sizes and hydrophilic coating thicknesses are constrained by the observed sizes and the modelled BC mass concentration as described by Kodros et al. (2018). These two states are illustrated in Fig. 2 of Kodros et al. (2018), where they are referred to as "rshell-constrained" (Fig. 2b) and "allCoreShell" (Fig. 2d). Particle mass, including BC mass, is conserved. The Allcore state is less realistic because every particle contains a BC core, whereas Arctic observations identify BC in roughly 10-20% of the particles (e.g. Sharma et al., 2017). As a result, the Allcore mixing assumption overestimates absorption (e.g. Alvarado et al., 2016). Rshell, which is based on observations, has a smaller fraction of coating material participating in absorption enhancement, resulting in lower absorption compared with Allcore; Rshell absorption is higher than that for the externally mixed assumption (Kodros et al., 2018). The Mie code of Bohren and Huffman (1983) for two concentric spheres is used to calculate $\sigma_{spt}$, $\sigma_{ap}$ and SSA.

Emissions are derived from the Emissions Database for Global Atmospheric Research (EDGAR) Hemispheric Transport of Air Pollution (HTAP) version 2.2 (Janssens-Maenhout et al., 2015). Following Xu et al. (2017), BC and organic carbon emissions from gas flaring derived from the Evaluating the Climate and Air Quality Impacts of short-lived Pollutants (ECLIPSE) emission inventory (Klimont et al., 2017) are included. Biomass burning emissions are from the Fire Inventory from NCAR (FINN) for the year 2015 (Wiedinmyer et al., 2011), but the particles are only injected into the boundary layer in this case. Dust emissions follow the DEAD scheme (Zender et al., 2003), and sea-salt aerosol emissions are based on Jaeglé et al. (2011). The model uses a refractive index for BC of 1.9+0.79i, as recommended by Bond and Bergstrom (2006). See Liu et al. (2020) for a review of the refractive index of BC. The refractive index differs from the value of 1.75+0.45i used by Kodros et al. (2018). That aside, details of the application of this version of the model to the Arctic as well as a detailed discussion of the role of mixing state on absorption by BC are given by Kodros et al (2018).

The data used here are from two vertical columns of the model: one column includes Axel Heiberg Island and the Arctic Ocean west of the island; the second is all Arctic Ocean to the west and slightly north of

Alert. Hereafter, the two grids are referred to as "Axel" and "NW Alert". They are centred on 78°N, 95°W and 86°N, 75°W, respectively, as indicated by the stars in Fig. 1. The model grid that includes Alert is not used in order to avoid problems that might be associated with modelling of the significant terrain of Ellesmere Island.

## 3 Results

In Section 3.1, we identify the strongest influences of dust on the $\sigma_{ap}$ observed from the POLAR 6. In section 3.2, we consider the mass absorption coefficients (MAC) for BC based on the observations (Alert and POLAR 6) and the model, including MAC at low BC mass concentrations. In Section 3.3, we present the profile data of rBC, median $\sigma_{ap}$, median SSA, $\sigma_{sp}$ as well as sulphate and organic mass concentrations, and compare with like quantities from the GEOS-Chem-TOMAS model. The regression between $\sigma_{ap}$ and rBC is used to increase the number of $\sigma_{ap}$ and SSA values, from which the medians are derived, enabling the influence of values below DL and during pressure changes to be better represented.

### 3.1 Dust absorption

Figure 2 shows the blue (450 nm), green (550 nm) and red (700 nm) $\sigma_{ap}$ plotted as a function of rBC for the nine POLAR 6 flights. A number of points in the rBC range of 0.15-0.3 μg $m^{-3}$ lie well above their respective linear regression lines. Those points represent measurements from two of the flights conducted out of Inuvik in plumes above 3 km with trajectories that trace back over Northern China and Mongolia. In Fig. 3, the scattering Ångström exponents for green-red wavelengths are plotted versus the number concentrations of particles larger than 2 μm. The Inuvik points are identified separately from the Alert and Eureka points, and the coarse particle influence associated with the Inuvik points is evident. The pattern of the lower Ångström exponent points (<0.8) versus increasing number concentrations of coarse particles agrees with the results of Hallar et al. (2015) for Asian dust measured at a mountain top in Colorado and with our general knowledge of aerosol optical properties (e.g. Aryal et al., 2014; Clarke et al., 2007; Russell et al., 2010). We assume the Inuvik points with a scattering Ångström exponent of less than 0.8 and coarse particle number concentrations greater than 0.5 $cm^{-3}$ are strongly influenced by dust.

The SSA from both the POLAR 6 and Alert are plotted against $\sigma_{sp}$ at 550 nm, in Fig. 4. The POLAR 6 points are from the POLAR 6 CLAP and Nephelometer measurements, and the dust-influenced points associated with the Inuvik flights are highlighted. The Alert data cover the period February, 2015 to April 14, 2015, when

the POLAR 6 left that region. Alert data from February and March of 2015 are included in part to provide a larger comparison base with the model and in part to demonstrate consistency of the POLAR 6 data with those from Alert, since the latter only reaches into the 0.75 $Mm^{-1}<\sigma_{ap}<1.6\ Mm^{-1}$ region during February. As in previous observations (e.g Targino et al., 2005; Andrews et al., 2011; Schmeisser et al., 2018), lower values of SSA are more frequent at these smaller $\sigma_{sp}$. Hereafter, we only consider data that fall into the region of green $\sigma_{sp}<15\ Mm^{-1}$, which represent 98% of the above-DL POLAR 6 data collected over Alert and Eureka and 85% of the above-DL Alert data (February to April 14, inclusive). With these constraints, strong contributions to $\sigma_{ap}$ from dust are removed. As next discussed, this improves the linear regression of $\sigma_{ap}$ with rBC.

### 3.2 Mass Absorption

The regression of $\sigma_{ap}$ with rBC for the combined POLAR 6 and Alert data (April 1-14), constrained as just discussed, has a slope of 18.4 $m^2g^{-1}$ and intercept of +0.15 (Fig. 5). In Fig. 5, separate regressions through the Alert data and through the POLAR 6 data overlap at a confidence level of greater than 95%. The $\sigma_{ap}$-rBC slope represents the average MAC of rBC in the measured particles, but this value is about twice that typically found for Arctic measurements at the green wavelength (e.g. 9.5 $m^2\ g^{-1}$, McNaughton et al., 2011; 8 $m^2\ g^{-1}$, Sharma et al., 2017; 9.8 $m^2\ g^{-1}$, Zanatta et al., 2018). Modelled $\sigma_{ap}$ are plotted against modelled BC for the NW Alert grid and Rshell mixing assumption in Fig. 6. These modelled values include a significant dust presence in many cases. We estimate the model MAC values for BC by constraining the dust concentrations to less than 0.2 $\mu g\ m^{-3}$, as shown by the black points in Fig. 6. For the case in Fig. 6, the MAC value for BC is 9.3 $m^2\ g^{-1}$. The modelled MAC value for BC is estimated at 13.1 $m^2\ g^{-1}$ for the NW Alert grid and Allcore mixing assumption. For the Axel grid, the estimated MAC value for BC is 8.8 $m^2\ g^{-1}$ for the Rshell assumption and 14.0 $m^2\ g^{-1}$ for the Allcore assumption. Due to a smaller influence of the coating material on absorption enhancement relative to the Allcore case, the lower Rshell results in a MAC value more consistent with those mentioned above.

We acknowledge that the model indicates a significant contribution from dust and possibly other non-BC components to atmospheric absorption in the Arctic. Average modelled profiles of the contributions to absorption from BC and the non-BC absorbing components of particles, assuming an external mixture, are shown in Fig. 7 for the NW Alert grid box, split between particles less than 700 nm diameter and particles greater than 700 nm diameter. The non-absorbing components include brown carbon and dust. For particles

smaller than 700 nm, the simulations suggest BC is on average the stronger absorbing component of the particles, with contributions from non-BC components approaching those from BC below 600 hPA. For particles larger than 700 nm, absorption by non-BC components, primarily dust, dominates in this model. As shown in Fig. 3, there were relatively few coarse particles were sampled from the POLAR 6 in the regions around Alert and Eureka, at any altitude, which represents a discrepancy between the observations and simulations.

The $\sigma_{ap}$-rBC regressions of the observations and the simulations have positive intercepts (regression-based confidence levels exceed 99.9%; the standard error of the intercepts, based on the measurement error, is 0.034). The intercepts are the result of increases in individual MAC values with decreasing concentrations of BC, as shown in Fig. 8a for the model and 8b for the observations. In these plots, MAC should be constant across all BC if absorption is solely due to BC without enhancements, such as lensing. The persistence of lower dust concentrations at low BC concentrations in the modelled MAC values (Fig. 8a) likely contributed to the increase in MAC at lower BC: as the BC concentrations decrease up to 100 times below the dust concentrations, absorption by dust with its lower imaginary refractive index (0.0065 in the model) may approach absorption by BC and increase the apparent MAC for BC. Because the modelled organic aerosol (OA) concentrations decrease proportionately with decreasing BC (Fig. 10 and 15) and the imaginary refractive index is lower (0.0065), absorbing OA cannot explain the increased MAC at lower BC. A relative increase in the coating thickness surrounding smaller BC cores at lower BC mass concentrations, as shown in Fig. 9, could also contribute to an increased enhancement factor. The observations suggest the presence of smaller amounts of potentially absorbing dust may be present at lower BC concentrations (Fig. 8b). The mass concentrations of coarse particles, estimated from the POLAR 6 size distributions assuming a density of 2 g $cm^{-3}$, are present across all rBC concentrations. We cannot distinguish whether the composition of these coarse particles is dust or sea salt, but, in accordance with the model, the observations suggest that dust may be a factor in the increasing MAC value at lower BC concentrations.

At higher BC concentrations, the MAC-vs-BC curves in Fig. 8 approach the MAC values determined from Fig. 5 for the observations (18.4 $m^2$ $g^{-1}$) and as in Fig. 6 for the model (8.8 $m^2$ $g^{-1}$ to 14.0 $m^2$ $g^{-1}$). Reasons for the higher observation-based MAC, based on the regression in Fig. 5, are unclear. There is no indication from the blue versus green slopes (Fig. 2) to suggest brown carbon is a significant factor for the Alert and Eureka data. Based on Figures 5-8, we estimate that dust may have contributed to the absorption in the amount of 0.15-0.3

$Mm^{-2}$. This estimate is significant, but not nearly sufficient to explain the differences in observed and modelled MAC. We consider three additional possibilities for the higher MAC:

1) The higher MAC is reasonable. This is suggested by the recent observations in smoke plumes and in background particles over the continental U.S.A. (Mason et al., 2018) as well as by Wu et al (2016) whose modelling of soot aggregates shows absorption by heavily-coated soot can be about 60% higher than uncoated soot. Another factor suggesting the higher MAC is reasonable is the close agreement between the present $\sigma_{ap}$ and SSA for Alert with the April summary of Schmeisser et al. (2018) for Alert: the ?ap are 0.50 $Mm^{-1}$ and 0.45 $Mm^{-1}$ for the present Alert analysis and for Schmeisser et al. (2018), respectively; the SSA are 0.95 and 0.95, respectively.
2) The higher observed MAC results from the overestimation of absorption by the filter-based measurements, as suggested by a number of observations. Lack et al. (2008) and Cappa et al. (2008a; 2008b) found that $\sigma_{abs}$ measured with a PSAP ranged from 1.3 to over two times higher than $\sigma_{abs}$ measured with a photoacoustic technique for organic mass (OM) concentrations above 2.5 $\mu g\ m^{-3}$ and the ratio of OM to the light absorbing component of the carbonaceous components exceeded about 15. To explain the absence of a similar effect on their results by ammonium sulphate particles, they suggested that the liquid nature of non-absorbing OM enhanced multiple scattering across the filter, further increasing absorption by particles on the filter. For the present measurements of rBC and OM (see Fig. 10 and 15), the ratio of OM to rBC (the only significant absorbing carbon) is estimated to be between 15 and 20, consistent with a strong impact of OM on our results. However, Lack et al. (2008) and Cappa et al. (2008a; 2008b) found that for relatively low (OM), the PSAP-based $\sigma_{abs}$ was only 12% higher than the photoacoustic-based $\sigma_{abs}$. At 1 $\mu g\ m^{-3}$ or less (Fig. 15), our flight OM concentrations fall well into the low OM concentration range of Cappa et al. (2008a; 2008b) and Lack et al. (2008). Also, consistent with the lowest level OM in Fig. 12, three years of OM measurements at Alert found OM always less than 0.5 $\mu g\ m^{-3}$ (Leaitch et al., 2018), suggesting that the average impact of this factor on our $\sigma_{abs}$ may be in the area of 12%. Considering the ambient temperatures (-40°C to -15°C), it is also possible that our non-absorbing OM was in solid forms (e.g. Zobrist et al., 2008), which might render its behavior on the filter more similar to ammonium sulphate. Sinha et al. (2017) studied the effect of volatile material (removed at 300°C) on absorption by particles at two Arctic sites. On

average and for particles less than 1 μm, they found that the absorption given by the PSAP was reduced by 22% with the removal of volatile material, which suggests that the present correction based on $\sigma_{sp}$ from the nephelometer may be insufficient.

3) The BC is underestimated here using rBC. Sharma et al. (2017) found that filter-based thermo-optical measurements of elemental carbon (EC) were an average of 1.9 times higher than rBC measured at Alert. This result will explain the high MAC value of 18.4 $m^2g^{-1}$, but there are many uncertainties associated with the measurement of BC by the many techniques, and the rBC measurement has been recommended for use (Bond et al., 2013). Schulz et al. (2019) estimate the deficiency in the POLAR 6 rBC mass concentrations due to sizing limitations at 7.5%, but they did not consider potential bias with respect to particle size. Accounting for size limitations of the rBC measurement at Alert increased the BC estimate by 40-50% during the spring measurement period (Sharma et al., 2017); although the resulting rBC was still a factor of 1.9 lower than the EC measurement.

If we assume that our observed $\sigma_{abs}$ are overestimated by 22% and our rBC are underestimated by 7.5%, the MAC value is reduced from 18.4 $m^2g^{-1}$ to about 13.4 $m^2g^{-1}$, which is similar to the modelled MAC values based on the Allcore assumption, but still about 50% higher than the more commonly accepted value of approximately 9 $m^2g^{-1}$ that is similar to the modelled value for the more realistic Rshell assumption. However, because there are a number of potential factors influencing the measurements of both $\sigma_{abs}$ and BC, we cannot attribute one value with the necessary certainty. In the following, we consider the measured $\sigma_{abs}$, which give the MAC value of 18.4 $m^2g^{-1}$, and values of $\sigma_{abs}$ divided by a factor of two (i.e. $\sigma_{abs}/2$) that gives a MAC value of 9.2 $m^2\ g^{-1}$, which is close to the more common MAC as well as the modelled MAC based on the Rshell assumption.

### 3.3 BC, Absorption, Scattering, SSA Vertical Distributions

We expand our dataset of $\sigma_{ap}$ values by employing the linear regression between $\sigma_{ap}$ and rBC shown in Fig. 5. This results in 956 $\sigma_{ap}$ points instead of 220, but because the linear relationship does not fully account for variations of individual points, we restrict the profiles of $\sigma_{ap}$ and SSA to median values calculated over approximately equal 50 hPa pressure intervals. Based on the linear fit, the uncertainty in the median $\sigma_{ap}$ is 6% at a 99% confidence level, but that excludes possible biases in either the measurement of $\sigma_{ap}$ or BC (as represented by rBC) discussed in Section 3.2. The corresponding uncertainty in the median SSA is ±0.01 or less

for the range of SSA discussed here, again excluding possible biases. As discussed in Section 2.1, the profile data, including $\sigma_{ap}$ and $\sigma_{ap}$ (SSA is dimensionless), have been adjusted to a standard temperature and pressure (20oC and 1013.25 hPa) for purposes of comparisons. We note that in-situ values of $\sigma_{ap}$ and $\sigma_{ap}$ are appropriate for calculating radiative effects.

Figure 10 shows vertical profiles of the rBC measurements of Schulz et al. (2018) and the modelled BC. Modelled BC for April 1-14 and rBC overlap well for pressures >900 hPa. In the pressure region of 600-900 hPa, the modelled BC is about a factor of two lower than the POLAR 6 rBC: median rBC is 0.043 μg $m^{-3}$; median modelled BC for April 1-14 is 0.022 μg $m^{-3}$. Using version 10.01 of GEOS-Chem (without TOMAS) and its adjoint, Xu et al. (2017) found that BC corresponding to these observations was dominated by sources from eastern and southern Asia. Xi et al. (2017) also found better agreement of modelled BC with these observations; although the same version of GEOS-Chem is used here, all biomass burning emissions were injected only within the boundary layer, potentially accounting for some of the lower modelled BC relative to rBC. The relative increase in rBC in the 600-900 hPa region is consistent with the mean profiles of McNaughton et al. (2011), and the median observed rBC concentration in the 600-900 hPa range is similar to the mode concentration of normally distributed values for "free tropospheric background haze" of 0.06 μg $m^{-3}$ estimated by Brock et al. (2011). Also, the lower part of the profile concentration data (<1 km) is similar to the springtime low-level profile BC concentrations from Ny-Ålesund measured by Ferrero et al. (2016). The present result is considerably lower than the medians of 0.1-0.5 μg $m^{-3}$ measured in the Arctic in 1983 (Hansen and Rosen, 1984), 1986 (Hansen and Novakov, 1989) and 1992 (Hansen et al., 1997). A decrease in BC at Alert, Nunavut, during the 1990s of more than 50% was associated with a reduction in Eurasian emissions (e.g. Sharma et al., 2019), and the present lower rBC concentrations near the surface may be connected to that reduction. Since east Asian emissions increased during the same time (e.g. van Donkelaar et al., 2008), it is difficult to assess the reason for the present lower concentrations in the 600-900 hPa range. It appears that the present observations mostly represent particles that spent a considerable length of time in the Arctic atmosphere.

Modelled profiles of $\sigma_{ap}$ for April 1-14 and both the Axel and NW Alert grids are shown in Fig. 11a and 11b for the Allcore and Rshell assumptions, respectively; major dust influence is removed, as in Fig. 6. The median values of the POLAR 6 rBC-based $\sigma_{ap}$, covering the period of April 7-13, inclusive, are also shown in Fig. 11 along with the hourly $\sigma_{ap}$ from Alert for April 1-14. The black POLAR 6 curves and Alert points are the measured values, and the red POLAR 6 curves and Alert points indicate the results for the measured values

divided by two or $\sigma_{ap}/2$. The median $\sigma_{ap}$ from the POLAR 6 agree reasonably with the corresponding Alert values. As expected, the modelled $\sigma_{ap}$ based on the Allcore assumption are overall higher than those based on the Rshell assumption. The simulated and observed $\sigma_{ap}$ exhibit opposite tendencies with pressure, except for pressures less than 600 hPa, where the model and POLAR 6 both suggest an increasing tendency of $\sigma_{ap}$ with decreasing pressure, consistent with Samset et al. (2013). Near the surface, the Allcore simulations are closer to the observed $\sigma_{ap}$ and the Rshell simulations are closer to the $\sigma_{ap}/2$. Between 800 hPa and 600 hPA, the modelled $\sigma_{ap}$, for both assumptions, overlap best with the observed $\sigma_{ap}/2$.

Vertical profiles of SSA are shown in Fig. 12. The modelled results are for February, 2015, March, 2015, and April 1-14, 2015 with the upper (a-c) and lower panels (d-f) representing the Allcore and Rshell assumptions, respectively. Median values of the Alert SSA, calculated from the measured $\sigma_{sp}$ and $\sigma_{ap}$, are shown for the corresponding model time period. The POLAR 6 SSA overlap well with the corresponding Alert SSA for April 1-14. The April 1-14 Alert SSA, based on the higher MAC, are the same as reported by Schmeisser et al. (2017) for Alert in April. The Alert SSA increase from February to April, which suggests a combination of the near-surface air cleansing itself of BC faster than the air in the lower troposphere during the high Arctic spring-to-summer transition and long-range transport aloft maintaining its influence longer than transport near the surface. Near the surface (>900 hPa), the modelled SSA are lower than the Alert and POLAR 6 results, in contrast to the modelled near-surface $\sigma_{ap}$ (Fig. 11). This difference is due to the modelled $\sigma_{sp}$ being overall lower than the observed $\sigma_{sp}$, as discussed below in connection with Fig. 13. In Fig. 12, the modelled and observation-based SSA have opposite tendencies from the surface to about 600 hPa. In the 700-800 hPa region, there is good agreement between the modelled SSA for the Rshell mixing state and the observation-based SSA for $\sigma_{ap}/2$. However, given that the modelled and measured $\sigma_{sp}$ are in reasonable agreement in that region (Fig. 13), the SSA agreement seems inconsistent with the underestimation by the model of BC in that pressure region (Fig. 10). The POLAR 6 near-surface (>950 hPa) and Alert SSA for early April range between 0.94 and 0.98, roughly consistent with the boundary layer SSA estimates of 0.97(+/-0.02) by Brock et al. (2011) and 0.95-0.96 by McNaughton et al. (2011). In the region of 600-900 hPa, the POLAR 6 SSA, based on $\sigma_{ap}/2$, range between 0.94 and 0.96, which is also consistent with McNaughton et al. (2011) in this region and the "free tropospheric background haze" estimate of Brock et al. (2011). However, the POLAR 6 SSA, based on $\sigma_{ap}$, range between 0.88 and 0.92 for the 600-900 hPa region, indicating substantially more absorption relative to scattering in this altitude range than found by Brock et al. (2011) and McNaughton et al. (2011). As mentioned above, the

ejection of biomass burning particles only into the boundary layer at the source may contribute to the higher modelled SSA in the 600-900 hPa layer.

Modelled $\sigma_{sp}$ for the April 1-14 period and observed $\sigma_{sp}$ are shown in Fig. 13a; only the model results for the Axel grid and Rshell assumption are shown, as those for the NW Alert grid are similar. The modelled and observed $\sigma_{sp}$ are most similar in the 600-900 hPa region, and therefore the differences between modelled and observation-based SSA (Fig. 12) in this pressure region are primarily the result of the variations in $\sigma_{ap}$ (Fig. 11). Close to the surface (>900 hPa), the April 1-14 modelled $\sigma_{sp}$ are lower than the POLAR 6 $\sigma_{sp}$ and at the low end of the Alert $\sigma_{sp}$, which contributes to the lower modelled SSA relative to the observation-based SSA in Fig. 10. Near the surface, the modelled $\sigma_{sp}$ for February agree best with the observed $\sigma_{sp}$, in part due to the higher submicron particle volumes simulated for February (Fig. 13b). The observed submicron volume concentrations are based on the UHSAS, and the modelled submicron volumes are calculated from the modelled mass concentrations of sulphate, organics and BC: (SO4/1.8 + Org/1.2 + BC/1.8), where 1.8, 1.2 and 1.8 are the respective densities of these components. The modelled scattering efficiency (scattering coefficient divided by volume concentration) is significantly lower than the efficiency based on the observations. Near the surface (>900 hPa), the median of $\sigma_{sp}$/Volume from the observations is 12.1 $\mu m^{-1}$ (range: 7.2-26.3) compared with 7.3 $\mu m^{-1}$ (range: 5.6-10.3) from the model. For the pressure interval of 600-900 hPa, the median of $\sigma_{sp}$/Volume from the observations is 10.8 $\mu m^{-1}$ (range: 6.2-36.4) versus 7.3 $\mu m^{-1}$ (range: 5.6-12.2) from the model. Model underestimation of submicron particle sizes may contribute to the lower modelled volume scattering efficiencies. In Fig. 14, the modelled particle size distributions for the Axel grid, April 1-14 period and averaged over the indicated pressure intervals are compared with measured distributions from the two flights (April 11 and 13) conducted in that grid. The modelled distributions for the 800-900 hPa and 900-1019 hPa intervals are shifted to slightly lower sizes relative to the average of the observations. The modelled distributions for 600-800 hPa are a closer match to the measurements, and for 400-600 hPa, the average of the modelled sizes is a reasonable match to the April 11 measurements, but exceeds the April 13 observations. The overall pattern is generally consistent with the variation of the modelled $\sigma_{sp}$, for the Axel grid and April 1-14 period, relative to the observed $\sigma_{sp}$, shown in Fig. 12a. In addition, the lower modelled volume scattering efficiencies may result from underestimation of the observed volumes that are based on the UHSAS.

The vertical distribution of the median concentrations of organic mass (OM) and sulphate mass (from Willis et al., 2018) are shown in Fig. 15 along with modelled organic and sulphate mass concentrations for the

Axel grid; results for the NW Alert grid are not appreciably different. The increase in rBC from the surface to about 650 hPa (Fig. 10) is paralleled by the increase in OM and its increase relative to sulphate. In Fig. 15, modelled OM near the surface (>900 hPa) is relatively close to the observed OM, but above that the observed OM is higher, by as much as a factor of two near 750 hPa. Near the surface, sulphate is underestimated by the model, which contributes to the model's lower volume and $\sigma_{sp}$ (Fig. 13) and hence SSA near the surface (Fig. 12).

**4. Discussion**

Models tend to underestimate Arctic BC (Bond et al., 2013; Eckhardt et al., 2015) and sulphate (Eckhardt et al., 2015). Emissions are an important aspect of such comparisons, and a recent study using the ECHAM model showed that improved emissions inventories increase the annual BC burden over the Arctic by up to 30% (Schacht et al., 2019). The vertical distributions in Fig. 10 and 15 suggest that the BC emissions are coupled with other carbonaceous emissions producing OM. In this case, the tendency of rBC/OM is to increase with altitude, from approximately 5.8% near the surface to 7.3% at 650 hPa; 5.8% is equivalent to the slope of the modelled result in Fig. 7d. Variations in source emissions and secondary organic aerosol formation will explain some of the increase in rBC/OM throughout this altitude range, but precipitation scavenging preferentially removing more organic material than BC is also a possibility. In the high Arctic, the number fractions of particles larger than 100 nm that contain detectable rBC are <30% (e.g. Sharma et al., 2017; Kodros et al., 2018; references therein), which means there is significant potential for nucleation scavenging to separate OM (and sulphate) from BC as part of the precipitation process. As discussed by Targino et al. (2006) and Andrews et al. (2011), this may contribute to the general reduction in SSA at lower $\sigma_{sp}$.

The microphysics of the rBC components also supports the importance of wet deposition to the present observations. Schulz et al. (2019) showed that the mass mean diameter of the rBC components decreases with decreasing pressure from the surface, with an increase in the number of rBC-containing particles explaining the higher rBC mass concentrations aloft. Wet deposition by convective clouds near the source regions will lead to smaller BC components of particles aloft, if the larger-sized BC components are scavenged on average more than smaller BC components nearer the emissions sources. The stronger emissions from more distant and southerly regions reaching higher altitudes (Stohl, 2006; Xu et al., 2017) could explain the general increase in rBC number concentrations with altitude. An important role for particle microphysics, and in particular the

representation of BC microphysics, in the modelling of BC transport to the Arctic is indicated. Despite the detailed microphysical model used here, the simulated BC vertical profiles suggest that the model transports more BC close to the surface. Excessive convective wet deposition that removes BC aloft (e.g. Mahmood et al., 2016) or re-distributes it to the near-surface region as well as the present modelled ejection of biomass burning particles only into the boundary layer are two potential reasons for the lower modelled BC in in this case. These results are consistent with Matsui et al. (2018), who point out that for models to properly simulate BC and its radiative impact on the Arctic atmosphere, they must have good representations of the microphysics and scavenging aspects of BC and other components of the aerosol. The results of Targino et al. (2005) and Andrews et al. (2011), suggesting lower SSA associated with lower $\sigma_{sp}$, as well as the present results are examples that wet scavenging may enhance the relative absorption by the Arctic aerosol. In addition, contributions from smaller amounts of dust at the lower BC in this case (Fig. 8) may also factor in the lower SSA at lower $\sigma_{sp}$.

Many studies have shown that BC may be of great importance to Arctic warming (e.g. Bond et al., 2013), and models compare better with ground-based observations in the Arctic than aloft (e.g. Eckhardt et al., 2015; present results). As discussed by Matsui et al. (2018) and indicated from the present work, representation of particle microphysics, including BC microphysics and scavenging of BC relative to all particles, is critical. There remains a need for focussed airborne studies conducting high quality and comprehensive measurements of BC microphysics and optical properties in the Arctic. Also, more knowledge of the BC mass absorption coefficient across the particle size spectrum is necessary if BC and its effects on absorption are to be properly assessed.

**5. Conclusions**

Relationships among vertically-distributed aerosol optical properties ($\sigma_{abs}$, $\sigma_{sp}$, and SSA), microphysics and particle chemistry were examined for a region of the Canadian archipelago between 79.9°N and 83.4°N from near the surface to 500 hPa. The airborne data were collected during April, 2015, and combined with ground-based observations from the observatory at Alert, Nunavut and simulations from the GEOS-Chem-TOMAS model (Kodros et al., 2018) in an effort to increase our knowledge of the effects of BC on absorption. The results were constrained for $\sigma_{sp}$ less than 15 $Mm^{-1}$, which represents 98% of the observed $\sigma_{sp}$, or the longer-lived Arctic haze in this case.

Large uncertainties in estimating $\sigma_{ap}$ and SSA are associated with this combined dataset. Based on observations from the POLAR 6 and Alert Observatory, the average mass absorption coefficient (MAC) for BC of 18.4 $m^2g^{-1}$ was much higher than the averaged modelled values of 13.6 $m^2\ g^{-1}$ and 9.1 $m^2\ g^{-1}$ (similar to some previous Arctic measurements) that represent different internal mixing assumptions discussed by Kodros et al. (2018). The higher MAC value may be due to a number of factors, including underestimation of BC, the presence of small amounts of dust, morphological arrangements of BC components within particles that are inconsistent with the often-used core-shell concept, and overestimation of $\sigma_{ap}$ by our observations. Due to the uncertainties, we compared $\sigma_{ap}$ and SSA against the modelled results using the values as measured and using values based on $\sigma_{ap}/2$ to provide a range consistent with the modelled MAC values.

Measured $\sigma_{abs}$, rBC and organic material in the particles all increased by close to a factor of two going from the surface to 750 hPa. Modelled BC, organics, and $\sigma_{ap}$ did not reflect the higher measured values in the 600-900 hPa region. The main sources of the differences between modelled and observed optical properties are the differences between the simulated and observed vertical distributions of rBC, organics and sulphate. As discussed, this highlights not only the importance of improving model emissions, deposition, and transport processes, but also microphysical details.

Assuming absorption overestimation, the SSA based on the POLAR 6 measurements ranged between 0.94 and 0.98, consistent with the results of Brock et al. (2011) and McNaughton et al. (2011). Assuming the measured MAC is reasonable, SSA ranged between 0.88 and 0.94, consistent with Schmeisser et al. (2017). The lower $\sigma_{sp}$ (<15 $Mm^{-1}$) constraint has been shown to yield lower SSA values on average (Targino et al., 2005; Andrews et al., 2011; this work). The relatively high frequency of occurrence of $\sigma_{sp}$ <15 $Mm^{-1}$ in this region of the Arctic during April makes it important to understand the size distributions and morphology of BC in particles at these lower $\sigma_{sp}$, the impact of smaller dust concentrations and to be able to simulate size-distributed wet scavenging of BC.

This work typifies the large uncertainty that exists in our knowledge of the contribution from BC to direct warming of the Arctic atmosphere. It suggests a lower level of confidence in assessing direct absorption by BC, and the need for more detailed efforts if the impact of BC on Arctic climate is to be properly established. Those efforts include improved measurements of BC and absorption, and more vertical profiles of aerosol chemistry, microphysics and optical properties.

Acknowledgements

NETCARE was funded by the Natural Sciences and Engineering Research Council (NSERC) of Canada under its Climate Change and Atmospheric Research program, with additional financial and in-kind support from Environment and Climate Change Canada, Fisheries and Oceans Canada, the Alfred Wegener Institute, the Major Research Project Management Fund at the University of Toronto, and the Deutsche Forschungsgemeinschaft (DFG, German Research Foundation) – project number 268020496 – TRR 172, within the Transregional Collaborative Research Center "ArctiC Amplification: Climate Relevant Atmospheric and SurfaCe Processes, and Feedback Mechanisms (AC)3". Colorado State University researchers were supported by the US Department of Energy's Atmospheric System Research, an Office of Science, Office of Biological and Environmental Research program, under grant no. DE-SC0011780, the US National Science Foundation, Atmospheric Chemistry program, under grant no. AGS-1559607, and by the US National Oceanic and Atmospheric Administration, an Office of Science, Office of Atmospheric Chemistry, Carbon Cycle, and Climate Program, under the cooperative agreement award no. NA17OAR430001. We gratefully acknowledge Kenn Borek Air Ltd, in particular our pilots and crew Garry Murtsell, Neil Traverse and Doug Mackenzie, for their support of our measurements. Logistical and technical support before and during the campaign was provided by a number of contributors, in particular by Desiree Toom (ECCC), Andrew Elford (ECCC), Dan Veber (ECCC), Julia Binder (AWI), Lukas Kandora (AWI), Jens Herrmann (AWI) and Manuel Sellmann (AWI). Extensive logistical and technical support was provided by Andrew Platt (ECCC), Mike Harwood (ECCC) and Martin Gerhmann (AWI). We are grateful to CFS Alert and Eureka Weather Station for supporting the measurements presented in this work.

References

- Adams, P. J. and Seinfeld, J. H.: Predicting global aerosol size distributions in general circulation models, J. Geophys. Res., 107, 4370, https://doi.org/10.1029/2001JD001010, 2002.
- Alvarado, M.J., Lonsdale, C.R., Macintyre, H.L., Bian, H., Chin, M., Ridley, D.A., Heald, C. L., Thornhill, K.L., Anderson, B.E., Cubison, M.J., Jimenez, J.L, Kondo, Y., Sahu, L.K., Dibb, J.E., and Wang, C.: Evaluating model parameterizations of submicron aerosol scattering and absorption with in situ data from ARCTAS 2008 Atmos. Chem. Phys., 16, 9435–9455, doi:10.5194/acp-16-9435-2016, 2016.
- Anderson, T. L. and Ogren, J. A.: Determining aerosol radiative properties using TSI 3563 integrating nephelometer, Aerosol Sci. Tech., 29, 57–69, 1998.
- Andrews, E., J.A. Ogren, P. Bonasoni, A. Marinoni, E. Cuevas, S. Rodriguez, J.Y. Sun, D. Jaffe, E. Fischer, U. Baltensperger, E. Weingartner, M. Collaud Coen, S. Sharma, A. Macdonald, W.R. Leaitch, N.-H. Lin, P. Laj, J.

Stamenov, I. Kalapov, A. Jefferson, P. Sheridan, Climatology of Aerosol Radiative Properties in the Free Troposphere. Atmospheric Research, 102, 365-393, doi:10.1016/j.atmosres.2011.08.017, 2011.

- Aryal, R. P., Voss, K. J., Terman, P. A., Keene, W. C., Moody, J. L., Welton, E. J., and Holben, B. N.: Comparison of surface and column measurements of aerosol scattering properties over the western North Atlantic Ocean at Bermuda, Atmos. Chem. Phys.,
- 14, 7617–7629, doi:10.5194/acp-14-7617-2014, 2014.
- Barrie, L. A.: Arctic air pollution: An overview of current knowledge, Atmos. Environ., 20, 643–663, doi:10.1016/0004-6981(86)90180-0, 1986.
- Barrie, L. A. and Hoff, R. M.: Five years of air chemistry observations in the Canadian Arctic. Atmos. Environ., 19, 1995-2010, 1985.
- Bigg E. K.: Comparison of aerosol at four baseline monitoring stations. J. appl. Met. 19, 521-523, 1980.
- Blanchet J.-P. and R. List: Estimation of optical properties of Arctic Haze using a numerical model, Atmos.-Ocean, 21, 444 – 464, 1987.
- Bohren, C. F. and Huffman, D. R.: Absorption and scattering of light by small particles, Wiley Interscience, New York, USA, 1983.
- Bond, T. C., Anderson, T. L., and Campbell, D.: Calibration and intercomparison of filter-based measurements of visible light absorption by aerosols, Aerosol Sci. Tech., 30, 582–600, 1999.
- Bond, T. C. and Bergstrom, R. W.: Light absorption by carbonaceous particles: an investigative review, Aerosol Sci. Tech., 40, 27–67, 2006.
- Bond, T. C., et al.: Bounding the role of black carbon in the climate system: A scientific assessment, J. Geophys. Res. Atmos., 118, 5380–5552, doi:10.1002/jgrd.50171, 2013.
- Brock, C. A., Cozic, J., Bahreini, R., Froyd, K. D., Middlebrook, A. M., McComiskey, A., Brioude, J., Cooper, O. R., Stohl, A., Aikin, K. C., de Gouw, J. A., Fahey, D. W., Ferrare, R. A., Gao, R.-S., Gore, W., Holloway, J. S., Hubler, G., Jefferson, A., Lack, D. A., Lance, S., Moore, R. H., Murphy, D. M., Nenes, A., Novelli, P. C., Nowak, J. B., Ogren, J. A., Peischl, J., Pierce, R. B., Pilewskie, P., Quinn, P. K., Ryerson, T. B., Schmidt, K. S., Schwarz, J. P., Sodemann, H., Spackman, J. R., Stark, H., Thomson, D. S., Thornberry, T., Veres, P., Watts, L. A., Warneke, C., and Wollny, A. G.: Characteristics, sources, and transport of aerosols measured in spring 2008 during the aerosol, radiation, and cloud processes affecting Arctic climate (ARCPAC) project, Atmos. Chem. Phys., 11, 2423–2453, doi:10.5194/acp-11-2423-2011, 2011.
- Clarke, A., McNaughton, C., Kapustin, V., Shinozuka, Y., Howell, S., Dibb, J., Zhou, J., Anderson, B., Brekhovskikh, V., Turner, H., and Pinkerton, M.: Biomass burning and pollution aerosol over North America: Organic components and their influence on spectral optical properties and humidification response, J. Geophys. Res., 112, D12S18, doi:10.1029/2006JD007777, 2007.
- Croft, B., Pierce, J.R., Martin, R.V., Hoose, C., Lohmann, U.: Uncertainty associated with convective wet removal of entrained aerosols in a global climate model, Atmospheric Chemistry and Physics, 12, 10725-10748, doi:10.5194/acp-12-10725-2012, 2012.
- Delene, D. and Ogren, J.A.: Variability of Aerosol Optical Properties at Four North American Surface Monitoring Sites. J. Atmos. Sci., 59, 1135-1150, 2002.
- Düsing, S., Wehner, B., Müller, T., Stöcker, A., and Wiedensohler, A.: The effect of rapid relative humidity changes on fast filter-based aerosol-particle light-absorption measurements: uncertainties and correction schemes, Atmos. Meas. Tech., 12, 5879–5895, doi.org/10.5194/amt-12-5879-2019, 2019.

- Dymarska, M., Murray, B. J., Sun, L., Eastwood, M. L., Knopf, D. A., and Bertram, A. K.: Deposition ice nucleation on soot at temperatures relevant for the lower troposphere, J. Geophys. Res., 111, D04204, doi:10.1029/2005JD006627, 2006.
- Eckhardt, S., Quennehen, B., Olivié, D.J.L., Berntsen, T.K., Cherian, R., Christensen, J. H., Collins, W., Crepinsek, S., Daskalakis, N., Flanner, M., Herber, A., Heyes, C., Hodnebrog, Ø., Huang, L., Kanakidou, M., Klimont, Z., Langner, J., Law, K.S., Lund, M.T., Mahmood, R., Massling, A., Myriokefalitakis, S., Nielsen, I.E., Nøjgaard, J.K., Quaas, J., Quinn, P.K., Raut, J.-C., Rumbold, S.T., Schulz, M., Sharma, S., Skeie, R.B., Skov, H., Uttal, T., von Salzen, K., and Stohl, A.: Current model capabilities for simulating black carbon and sulfate concentrations in the Arctic atmosphere: a multi-model evaluation using a comprehensive measurement data set, Atmos. Chem. Phys., 15, 9413–9433, doi:10.5194/acp-15-9413-2015, 2015.
- Ferrero, L., Cappelletti, D., Busetto, M., Mazzola, M., Lupi, A., Lanconelli, C., Becagli, S., Traversi, R., Caiazzo, L., Giardi, F., Moroni, B., Crocchianti, S., Fierz, M., Močnik, G., Sangiorgi, G., Perrone, M. G., Maturilli, M., Vitale, V., Udisti, R., and Bolzacchini, E.: Vertical profiles of aerosol and black carbon in the Arctic: a seasonal phenomenology along 2 years (2011–2012) of field campaigns, Atmos. Chem. Phys., 16, 12601–12629, https://doi.org/10.5194/acp-16-12601-2016, 2016.
- Fisher, J. A., Jacob, D. J., Wang, Q., Bahreini, R., Carouge, C. C., Cubison, M. J., Dibb, J. E., Diehl, T., Jimenez, J. L., Leibensperger, E. M., Lu, Z., Meinders, M. B. J., Pye, H. O. T., Quinn, P. K., Sharma, S., Streets, D. G., van Donkelaar, A., and Yantosca, R. M.: Sources, distribution, and acidity of sulfate-ammonium aerosol in the Arctic in winter-spring, Atmos. Environ., 45, 7301-7318, doi:10.1016/j.atmosenv.2011.08.030, 2011.
- Flanner, M., Zender, C., Randerson, J. and Rasch, P.: Present-day climate forcing and response from black carbon in snow, J. Geophys. Res., 112, D11202, doi:10.1029/2006JD008003, 2007.
- Gysel, M., Laborde, M., Olfert, J. S., Subramanian, R., and Gröhn, A. J.: Effective density of Aquadag and fullerene soot black carbon reference materials used for SP2 calibration, Atmos. Meas. Tech., 4, 2851–2858, https://doi.org/10.5194/amt-4-2851-2011, 2011.
- Hallar, A.G., R. Petersen, E. Andrews, J. Michalsky, I. B. McCubbin, and J. A. Ogren: Contributions of dust and biomass burning to aerosols at a Colorado mountain-top site, Atmos. Chem. Phys., 15, 13665–13679, doi:10.5194/acp-15-13665-2015, 2015.
- Hansen, A.D.A. and Rosen, H. : Vertical distribution of particulate carbon, sulfur, and bromine in the Arctic haze and comparison with ground-level measurements at Barrow, Alaska, Geophys. Res. Lett., 11, 381-384, 1984.
- Hansen, A.D.A. and Rosen, H. : Horizontal inhomogeneities in the particulate carbon component of the Arctic haze, Atmos. Environ., 19, 2175-2180, 1985.
- Hansen, A.D.A and Novakov, T. : Aerosol black carbon measurements in the Arctic haze during AGASP-II. J. Atmos. Chem., 9, 347-361, 1989.
- Hansen, A.D.A., Polissar, A.V., Schnell, R.C.: Airborne aerosol and black carbon measurements over the East Siberian Sea, spring 1992, Atmos. Res., 44, 1534-166, 1997.
- Hansen, J., and L. Nazarenko: Soot climate forcing via snow and ice albedos, Proc. Natl. Acad. Sci. U. S. A., 101, 423 – 428, doi:10.1073/pnas.2237157100, 2004.
- Heintzenberg J.: Particle size distribution and optical properties-of Arctic haze. Tellus 32, 251-260, 1980.
- Heidam, N. Z., Wåhlin, P., and Christensen, J.H.: Tropospheric gases and aerosols in northeast Greenland, J. Atmos. Sci., 56, 261-278, 1999.

- Hess, M., Koepke, P. and Schult, I.: Optical Properties of Aerosols and Clouds: The Software Package OPAC, Bulletin American Meteor. Soc., 79(5), 831–844, doi:https://doi.org/10.1175/1520-0477(1998)079<0831:OPOAAC>2.0.CO;2, 1998.
- Hirdman, D., Burkhart, J. F., Sodemann, H., Eckhardt, S., Jefferson, A., Quinn, P.K., Sharma, S., Ström, J., and Stohl, A.: Long-term trends of black carbon and sulphate aerosol in the Arctic: changes in atmospheric transport and source region emissions, Atmos. Chem. Phys., 10, 9351–9368, doi:10.5194/acp-10-9351-2010, 2010.
- Holmgren B., Shaw G. E. and Weller G.: Turbidity in the Arctic atmosphere, AIDJEX Bull., 27, 135-148, 1974.
- Jaeglé, L., Quinn, P. K., Bates, T. S., Alexander, B., and Lin, J.-T.: Global distribution of sea salt aerosols: new constraints from in situ and remote sensing observations, Atmos. Chem. Phys., 11, 3137–3157, https://doi.org/10.5194/acp-11-3137-2011, 2011.
- Janssens-Maenhout, G., Crippa, M., Guizzardi, D., Dentener, F., Muntean, M., Pouliot, G., Keating, T., Zhang, Q., Kurokawa, J., Wankmüller, R., Denier van der Gon, H., Kuenen, J. J. P., Klimont, Z., Frost, G., Darras, S., Koffi, B., and Li, M.: HTAP_v2.2: a mosaic of regional and global emission grid maps for 2008 and 2010 to study hemispheric transport of air pollution, Atmos. Chem. Phys., 15, 11411–11432, https://doi.org/10.5194/acp-15-11411-2015, 2015.
- Kahnert, M.: On the Discrepancy between Modeled and Measured Mass Absorption Cross Sections of Light Absorbing Carbon Aerosols, Aerosol Science and Technology, 44:6, 453-460, doi: 10.1080/02786821003733834, 2010.
- Kim, J., Bauer, H., Dobovičnik, T., Hitzenberger, R., Lottin, D., Ferry, D. and Petzold, A.: Assessing Optical Properties and Refractive Index of Combustion Aerosol Particles Through Combined Experimental and Modeling Studies, Aerosol Science and Technology, 49, 340-350, doi: 10.1080/02786826.2015.1020996, 2015.
- Klimont, Z., Kupiainen, K., Heyes, C., Purohit, P., Cofala, J., Rafaj, P., Borken-Kleefeld, J., and Schöpp, W.: Global anthropogenic emissions of particulate matter including black carbon, Atmos. Chem. Phys., 17, 8681–8723, https://doi.org/10.5194/acp-17-8681-2017, 2017.
- Kodros, J. K., Hanna, S., Bertram, A., Leaitch, W. R., Schulz, H., Herber, A., Zanatta, M., Burkart, J., Willis, M., Abbatt, J. 20 P. D. and Pierce, J. R.: Size-resolved mixing state of black carbon in the Canadian high Arctic and implications for simulated direct radiative effect, Atmospheric Chemistry and Physics Discussions, 1–32, doi:https://doi.org/10.5194/acp-2018-171, 2018.
- Kopke, P., Hess, M., Schult, I., and Shettle, E. P.: Global Aerosol Data Set, Max Planck Inst. für Meteorol., Hamburg, Germany, 1997.
- Kopp, R. E. and Mauzerall, D. L.: Assessing the climatic benefits of black carbon mitigation, P. Natl. Acad. Sci. USA, 107, 11703–11708, doi:10.1073/pnas.0909605107, 2010.
- Laborde, M., Mertes, P., Zieger, P., Dommen, J., Baltensperger, U., and Gysel, M.: Sensitivity of the Single Particle Soot Photometer to different black carbon types, Atmos. Meas. Tech., 5, 1031–1043, https://doi.org/10.5194/amt-5-1031-2012, 2012.
- Lack, D. A., C. D. Cappa, D. S. Covert, T. Baynard, P. Massoli, B. Sierau, T. S. Bates, P. K. Quinn, E. R. Lovejoy, and A. R. Ravishankara (2008), Bias in filter-based aerosol light absorption measurements due to organic aerosol loading: Evidence from ambient measurements, Aerosol Sci. Technol., 42(12), 1033–1041.
- Law, K. S. and Stohl, A.: Arctic air pollution: origins and impacts. Science, 315, 1537–1540, 2007.

- Leaitch, W.R., Hoff, R.M., and MacPherson, J.I.: Airborne and lidar measurements of aerosol and cloud particles in the troposphere over Alert Canada in April 1986. J. Atmos. Chem., 9, 187-211, 1989.
- Leaitch, W.R., S. Sharma, L. Huang, A. M. Macdonald, D. Toom-Sauntry, A. Chivulescu, K. von Salzen, J.R. Pierce, N.C. Shantz, A. Bertram, J. Schroder, A.-L. Norman, R.Y.-W. Chang: Dimethyl Sulphide Control of the Clean Summertime Arctic Aerosol and Cloud, Elementa: Science of the Anthropocene 1: 000017, doi: 10.12952/journal.elementa.000017, 2013.
- Leaitch, W. R., L. M. Russell, J. Liu, F. Kolonjari, D. Toom, L. Huang, S. Sharma, A. Chivulescu, D. Veber, and W. Zhang: Organic functional groups in the submicron aerosol at 82.5 N, 62.5W from 2012 to 2014, Atmos. Chem. Phys., 18, 1–19, doi.org/10.5194/acp-18-1-2018, 2018.
- Lee, Y. H. and Adams, P. J.: A Fast and Efficient Version of the TwO-Moment Aerosol Sectional (TOMAS) Global Aerosol Microphysics Model, Aerosol Sci. Technol., 46, 678–689, https://doi.org/10.1080/02786826.2011.643259, 2012.
- Lee, Y. H., Pierce, J. R., and Adams, P. J.: Representation of nucleation mode microphysics in a global aerosol model with sectional microphysics, Geosci. Model Dev., 6, 1221–1232, https://doi.org/10.5194/gmd-6-1221-2013, 2013.
- Leighton, H.: Influence of the Arctic Haze on the solar radiation budget. Atmos. Environ., 17, 2065-2068, 1983.
- Liu, F., Yon, J., Fuentes, A., Lobo, P., Smallwood, G.J. and Corbin, J.C.: Review of recent literature on the light absorption properties of black carbon: Refractive index, mass absorption cross section, and absorption function, Aerosol Science and Technology, 54, doi.org/10.1080/02786826.2019.1676878, 2020.
- Mahmood, R., Salzen, K., Flanner, M., Sand, M., Langner, J.,Wang, H., and Huang, L.: Seasonality of global and Arctic black carbon processes in the Arctic Monitoring and Assessment Programme models, J. Geophys. Res.-Atmos., 121, 7100–7116, 2016.
- Mason, B., Wagner, N.L., Adler, G., Andrews, E., Brock, C.A., Gordon, T.D., Lack, D.A., Perring, A.E., Richardson, M.S., Schwarz, J.P., Shook, M.A., Thornhill, K.L., Ziembad, L.D., and Murphy, D.M.: An intercomparison of aerosol absorption measurements conducted during the SEAC4RS campaign, Aerosol Sci. & Technol., 52, 1012–1027, doi.org/10.1080/02786826.2018.1500012, 2018.
- Matsui, H., Hamilton, D.S., and Mahowald, N.M.: Black carbon radiative effects highly sensitive to emitted particle size when resolving mixing-state diversity, Nat. Commun., doi: 10.1038/s41467-018-05635-1, 2018.
- McNaughton, C. S., A. D. Clarke, S. Freitag, V. N. Kapustin, Y. Kondo, N. Moteki, L. Sahu, N. Takegawa, J. P. Schwarz, J. R. Spackman, L. Watts, G. Diskin, J. Podolske, J. S. Holloway, A. Wisthaler, T. Mikoviny, J. de Gouw, C. Warneke, J. Jimenez, M. Cubison, S. G. Howell, A. Middlebrook, R. Bahreini, B. E. Anderson, E. Winstead, K. L. Thornhill, D. Lack, J. Cozic, and C. A. Brock (2011), Absorbing aerosol in the troposphere of the Western Arctic during the 2008 ARCTAS/ARCPAC airborne field campaigns, Atmospheric Chemistry and Physics, 11(15), 7561–7582, doi: 10.5194/acp-11-7561-2011.
- McConnell, J. R., Edwards, E., Kok, G. L., Flanner, M. G., Zender, C. S., Saltzman, E. S., Banta, J. R., Pasteris, D. R., Carter, M. M., and Kahl, J. D.: 20th-century industrial black carbon emissions altered Arctic climate, Science, 317, 1381–1384, 2007.
- Markowicz, K.M.,Ritter, C., Lisoka, J., Makuch, P., Stachlewska, S., Cappelletti, D., Mazzola, M., Chilinski, M. T.: Vertical variability of aerosol single-scattering albedo and equivalent black carbon concentration based on in-situ and remote sensing techniques during the iAREA campaigns in Ny-Ålesund, Atmos. Environ., 164, 431-447, https://doi.org/10.1016/j.atmosenv.2017.06.014, 2017.

- Mitchell M.: Visual range in the polar regions with particular reference to the Alaskan Arctic. J. Atmos. Terr. Phys., Special Supplement, 195-211, 1956.Moteki, N. and Kondo, Y.: Effects of mixing state on black carbon measurements by laser-induced incandescence, Aerosol Sci. Technol., 41, 398–417, https://doi.org/10.1080/02786820701199728, 2007.
- Moteki, N. and Kondo, Y.: Dependence of laser-induced incandescence on physical properties of black carbon aerosols: measurements and theoretical interpretation, Aerosol Sci. Tech., 44, 663–675, https://doi.org/10.1080/02786826.2010.484450, 2010.
- Najafi, M. R., Zwiers, F. W. and Gillett, N. P.: Attribution of Arctic temperature change to greenhouse-gas and aerosol 25 influences, Nature Clim. Change, 5(3), 246–249, doi:10.1038/nclimate2524, 2015.
- Navarro, J. C. A., Varma, V., Riipinen, I., Seland, Ø., Kirkevåg, A., Struthers, H., Iversen, T., Hansson, H.-C. and Ekman, A. M. L.: Amplification of Arctic warming by past air pollution reductions in Europe, Nature Geoscience, 9(4), 277–281, 30 doi:10.1038/ngeo2673, 2016.
- Ogren, J. A.: Comment on "Calibration and intercomparison of filter-based measurements of visible light absorption by aerosols", Aerosol Sci. Tech., 44, 589–591, 1608, doi.org/10.1080/02786826.2010.482111, 2010.
- Ogren, J.A., Wendell, J., Andrews, E., et al.:"Continuous Light Absorption Photometer for Long-Term Studies," Atmos Meas. Tech.,10, 4805-4818, doi:10.5194/amt-10-4805-2017, 2017.Pluchino A. B., Goldberg S. S., Dowling J. M. and Randall C. M: Refractive index measurements of single micron-sized carbon particles. Appl. Opt. 19, 3370-3372, 1980.
- Pueschel, R.F. and S.A. Kinne: Physical and radiative properties of Arctic atmospheric aerosols, Sci. Tot. Environ., 161, 811-824, 1995.
- Qi, L., Q. Li, D. K. Henze, H.-L. Tseng, and C. He: Sources of springtime surface black carbon in the Arctic: an adjoint analysis for April 2008, Atmos. Chem. Phys., 17, 9697–9716, doi:10.5194/acp-17-9697-2017, 2017.
- Quinn, P. K. and Coauthors, 2008: Short-lived pollutants in the Arctic: their climate impact and possible mitigation strategies. Atmos. Chem. Phys., 8(6), doi:10.5194/acp-8-1723-2008.
- Quinn, P.K., T. S. Bates, K. Schulz, and G. E. Shaw: Decadal trends in aerosol chemical composition at Barrow, Alaska: 1976–2008, Atmos. Chem. Phys., 9, 8883–8888, 2009.
- Radke L. F., Lyons J. H., Hegg D. A., Hobbs P. V. and Bailey I. H.: Airborne observations of Arctic aerosols-I. Characteristics of Arctic haze, Geophys. Res. Lett. 11, 393-396, 1984.
- Rahn K. A., Boyrs R. and Shaw G. E.: The Asian source of Arctic haze bands, Nature, 268, 713-715, 1977.
- Rahn K. A.: The Arctic air-sampling network in 1980, Atmos. Environ., 15, 1349-1352, 1981.
- Russell, P. B., Bergstrom, R. W., Shinozuka, Y., Clarke, A. D., De-Carlo, P. F., Jimenez, J. L., Livingston, J. M., Redemann, J., Dubovik, O., and Strawa, A.: Absorption Angstrom Exponent in AERONET and related data as an indicator of aerosol composition, Atmos. Chem. Phys., 10, 1155–1169, doi:10.5194/acp-10-1155-2010, 2010.
- Samset, B. H., Myhre, G., Schulz, M., Balkanski, Y., Bauer, S., Berntsen, T. K., Bian, H., Bellouin, N., Diehl, T., Easter, R. C., Ghan, S. J., Iversen, T., Kinne, S., Kirkevåg, A., Lamarque, J.-F., Lin, G., Liu, X., Penner, J. E., Seland, Ø., Skeie, R. B., Stier, P., Takemura, T., Tsigaridis, K., and Zhang, K.: Black carbon vertical profiles strongly affect its radiative forcing uncertainty, Atmos. Chem. Phys., 13, 2423-2434, https://doi.org/10.5194/acp-13-2423-2013, 2013.

- Sand, M., Berntsen, T. K., von Salzen, K., Flanner, M. G., Langner, J., and Victor, D. G: Response of the Arctic temperature to changes in emissions of short-lived climate forcers, Nat. Clim. Chang., 6, 286–289, https://doi.org/10.1038/nclimate2880, 2016.
- Schacht, J., Heinold, B., Quaas, J., Backman, J., Cherian, R., Ehrlich, A., Herber, A., Huang, W. T. K., Kondo, Y., Massling, A., Sinha, P. R., Weinzierl, B., Zanatta, M., and Tegen, I.: The importance of the representation of air pollution emissions for the modeled distribution and radiative effects of black carbon in the Arctic, Atmos. Chem. Phys. Discuss., https://doi.org/10.5194/acp-2019-71, in review, 2019.
- Schmeisser, L., Backman, J., Ogren, J. A., Andrews, E., Asmi, E., Starkweather, S., Uttal, T., Fiebig, M., Sharma, S., Eleftheriadis, K., Vratolis, S., Bergin, M., Tunved, P., and Jefferson, A.: Seasonality of aerosol optical properties in the Arctic, Atmos. Chem. Phys. 18, 11599-11622, doi:10.5194/acp-18-11599-2018, 2018.
- Schnell R. C. and Raatz W. E.: Vertical and horizontal characteristics of Arctic hare during AGASP; Alaskan Arctic, Geophys. Res. Lett. 11, 369-376, 1984.
- Schulz, H., Bozem, H., Zanatta, M., Leaitch, W. R., Herber, A. B., Burkart, J., Willis, M. D., Hoor, P. M., Abbatt, J. P. D. and Gerdes, R.: High–Arctic aircraft measurements characterising black carbon vertical variability in spring and summer, 35 Atmospheric Chemistry and Physics Discussions, 1–34, doi:10.5194/acp-2018-587, 2018.
- Schwarz, J. P., Spackman, J. R., Gao, R. S., Watts, L. A., Stier, P., Schulz, M., Davis, S. M., Wofsy, S. C. and Fahey, D. W.: Global-scale black carbon profiles observed in the remote atmosphere and compared to models, Geophys. Res. Lett., 37, L18812, doi:10.1029/2010GL044372, 2010.
- Sirois, A., and L. A. Barrie: Arctic lower tropospheric aerosol trends and composition at Alert, Canada: 1980–1995, J. Geophys. Res., 104, 11,599–11,618, doi:10.1029/1999JD900077, 1999.
- Sharma, S., D. Lavoue, H. Cachier, L. A. Barrie, and S. L. Gong: Long-term trends of the black carbon concentrations in the Canadian Arctic, J. Geophys. Res., 109, D15203, doi:10.1029/2003JD004331, 2004.
- Sharma, S., E. Andrews, L. A. Barrie, J. A. Ogren, and D. Lavoue´: Variations and sources of the equivalent black carbon in the high Arctic revealed by long-term observations at Alert and Barrow: 1989–2003, J. Geophys. Res., 111, D14208, doi:10.1029/2005JD006581, 2006.
- Sharma, S., M. Ishizawa, D. Chan, D. Lavoue´, E. Andrews, K. Eleftheriadis, and S. Maksyutov: 16-Year Simulation of Arctic Black Carbon: Transport, Source Contribution, and Sensitivity Analysis on Deposition, J. Geophys. Res., 118, doi:10.1029/2012JD017774, 2013.
- Sharma, S., W. R. Leaitch, L. Huang, D. Veber, F. Kolonjari, W. Zhang, S. J. Hanna, A. K. Bertram, and J. A. Ogren: An evaluation of three methods for measuring black carbon in Alert, Canada, Atmos. Chem. Phys., 17, 15225–15243, doi.org/10.5194/acp-17-15225-2017, 2017.
- Sharma, S., Barrie, L. A., Magnusson, E., Brattström, G., Leaitch, W. R., Steffen, A., & Landsberger, S. (2019). A factor and trends analysis of multidecadal lower tropospheric observations of Arctic aerosol composition, black carbon, ozone, and mercury at Alert, Canada, J. Geophys. Res.: Atmos., 124. https://doi.org/10.1029/2019JD030844, 2019.
- Shaw, G. E.: Evidence for a central Eurasian source area of Arctic haze in Alaska, Nature, 299, 815–818, 1983.
- Sherman, J. P., Sheridan, P. J., Ogren, J. A., Andrews, E., Hageman, D., Schmeisser, L., Jefferson, A., and Sharma, S.: A multi-year study of lower tropospheric aerosol variability and systematic relationships from

four North American regions, Atmos. Chem. Phys., 15, 12487–12517, https://doi.org/10.5194/acp-15-12487-2015, 2015.

- Shindell, D. and G. Faluvegi: Climate response to regional radiative forcing in the twentieth century. Nature Geosci., 2(4), 294-300, doi: 10.1038/NGEO473, 2009.
- Sinha, P. R., Kondo, Y., Koike, M., Ogren, J. A., Jefferson, A., Barrett, T. E., Sheesley, R. J., Ohata, S., Moteki, N., Coe, H., Liu, D., Irwin, M., Tunved, P., Quinn, P. K., and Zhao, Y.: Evaluation of ground-based black carbon measurements by filter-based photometers at two Arctic sites, J. Geophys. Res. Atmos., 122, 3544–3572, doi:10.1002/2016JD025843, 2017.
- Slowik, J. G., Cross, E. S., Han, J.-H., Davidovits, P., Onasch, T. B., Jayne, J. T., Williams, L. R., Canagaratna, M. R., Worsnop, D. R., Chakrabarty, R. K., Moosmüller, H., Arnott, W. P., Schwarz, J. P., Gao, R.-S., Fahey, D. W., Kok, G. L., and Petzold, A.: An Inter-Comparison of Instruments Measuring Black Carbon Content of Soot Particles, Aerosol Sci. Technol., 41, 295–314, https://doi.org/10.1080/02786820701197078, 2007.
- Sinha, P. R., Y. Kondo, M. Koike, J. A. Ogren, A. Jefferson, T. E. Barrett, R. J. Sheesley, S. Ohata, N. Moteki, H. Coe, D. Liu , M. Irwin, P. Tunved, P. K. Quinn, and Y. Zhao: Evaluation of ground-based black carbon measurements by filter-based photometers at two Arctic sites, J. Geophys. Res. Atmos., 122, 3544–3572, doi:10.1002/2016JD025843, 2017.
- Sobhani, N., Kulkarni, S., and Carmichael, G.R.: Source sector and region contributions to black carbon and PM2:5 in the Arctic, Atmos. Chem. Phys., 18, 18123–18148, doi.org/10.5194/acp-18-18123-2018, 2018.
- Spackman, J. R., Gao, R. S., Neff, W. D., Schwarz, J. P., Watts, L. A., Fahey, D. W., Holloway, J. S., Ryerson, T. B., Peischl, J., and Brock, C. A.: Aircraft observations of enhancement and depletion of black carbon mass in the springtime Arctic, Atmos. Chem. Phys., 10, 9667–9680, https://doi.org/10.5194/acp-10-9667-2010, 2010.
- Staebler, R.M., G. den Hartog, B. Georgi, and Thorsten Düsterdiek: Aerosol size distributions in Arctic haze during the POLAR Sunrise Experiment 1992, J. Geophys. Res., 99, 25,429-25,437, 1994.
- Stohl, A., Aamaas, B., Amann, M., Baker, L. H., Bellouin, N., Berntsen, T. K., Boucher, O., Cherian, R., Collins, W., Daskalakis, N., Dusinska, M., Eckhardt, S., Fuglestvedt, J. S., Harju, M., Heyes, C., Hodnebrog, Ø., Hao, J., Im, U., Kanakidou, M., Klimont, Z., Kupiainen, K., Law, K. S., Lund, M. T., Maas, R., MacIntosh, C. R., Myhre, G., Myriokefalitakis, S., Olivié, D., Quaas, J., Quennehen, B., Raut, J.-C., Rumbold, S. T., Samset, B. H., Schulz, M., Seland, Ø., Shine, K. P., Skeie, R. B., Wang, S., Yttri, K. E., and Zhu, T.: Evaluating the climate and air quality impacts of short-lived pollutants, Atmos. Chem. Phys., 15, 10529-10566, https://doi.org/10.5194/acp-15-10529-2015, 2015.
- Targino, A.C., Noone, K.J., Ostrom, E: Airborne in-situ characterization of dry aerosol optical properties in a multisource influenced marine region, Tellus 57B, 247–260, 2005.
- Valero F. P. J., Ackerman T. P. and Gore J. Y.: The absorption of solar radiation by the Arctic atmosphere during the haze season and its effects on the radiation balance. Geophys. Res. Lett. 11, 465-468, 1984.
- Valero, F.P.J., T.P. Ackerman, and W.J.R. Gore: The effects of the arctic haze as determined from airborne radiometric measurements during AGASP II, J. Atmos. Chem., 9, 225-244, 1989.
- van Donkelaar, A., Martin, R. V., Leaitch, W. R., Macdonald, A. M., Walker, T. W., Streets, D.G., Zang, Q., Dunlea, E., Jimenez, J. L., Dibb, J. E., Huley, G., Weber, R., and Andreae, M.O. 2008: Analysis of Aircraft and Satellite Measurements from the Intercontinental Chemical Transport Experiment (INTEX-B) to Quantify Long-Range Transport of Asian Sulfur to North America, Atmos. Chem. Phys., 8, 2999-3014, www.atmos-chem-phys.net/8/2999/2008/, 2008.

- Wiedinmyer, C., Akagi, S. K., Yokelson, R. J., Emmons, L. K., Al-Saadi, J. A., Orlando, J. J., and Soja, A. J.: The Fire Inventory from NCAR (FINN): a high-resolution global model to estimate the emissions from open burning, Geosci. Model Dev., 4, 625–641, https://doi.org/10.5194/gmd-4-625-2011, 2011.
- Willis, M.D., Bozem, H., Kunkel, D., Lee, A.K.Y., Schulz, H., Burkart, J., Aliabadi, A.A., Herber, A.B., Leaitch, W.R., and Abbatt, J.P.D.: Aircraft-based measurements of High Arctic springtime aerosol show evidence for vertically varying sources, transport and composition, Atmos. Chem. Phys., 19, 57–76, https://doi.org/10.5194/acp-19-57-2019, 2019.
- Wofsy, S. C., The HIPPO Science Team and Cooperating Modellers and Satellite Teams: HIAPER Pole-to-Pole Observations (HIPPO): fine-grained, global-scale measurements of climatically important atmospheric gases and aerosols, Phil. Trans. R. Soc. A (2011) 369, 2073–2086, doi:10.1098/rsta.2010.0313, 2011.
- Xu, J.-W., Martin, R. V., Morrow, A., Sharma, S., Huang, L., Leaitch, W. R., Burkart, J., Schulz, H., Zanatta, M., Willis, M. D., Henze, D. K., Lee, C. J., Herber, A. B. and Abbatt, J. P. D.: Source attribution of Arctic black carbon constrained by aircraft and surface measurements, Atmospheric Chemistry and Physics, 17, 11971–11989, doi:10.5194/acp-17-11971-2017, 2017.
- Yu, H., Li, W., Zhang, Y., Tunved, P., Dall'Osto, M., Shen, X., Sun, J., Zhang, X., Zhang, J., and Shi, Z.: Organic coating on sulfate and soot particles during late summer in the Svalbard Archipelago, Atmos. Chem. Phys., 19, 10433–10446, https://doi.org/10.5194/acp-19-10433-2019, 2019.
- Zanatta, M., Paolo Laj, Martin Gysel, Urs Baltensperger, Stergios Vratolis, Konstantinos Eleftheriadis, Yutaka Kondo, Philippe Dubuisson, Victor Winiarek, Stelios Kazadzis, Peter Tunved and Hand-Werner Jacobi: Effects of mixing state on optical and radiative properties of black carbon in the European Arctic, Atmos. Chem. Phys. Discuss., https://doi.org/10.5194/acp-2018-455, 2018.
- Zender, C. S.: Mineral Dust Entrainment and Deposition (DEAD) model: Description and 1990s dust climatology, J. Geophys. Res., 108, 4416, https://doi.org/10.1029/2002JD002775, 2003.
- Zobrist, B., Marcolli, C., Pedernera, D. A., and Koop, T.: Do atmospheric aerosols form glasses?, Atmos. Chem. Phys., 8, 5221-5244, https://doi.org/10.5194/acp-8-5221-2008, 2008.

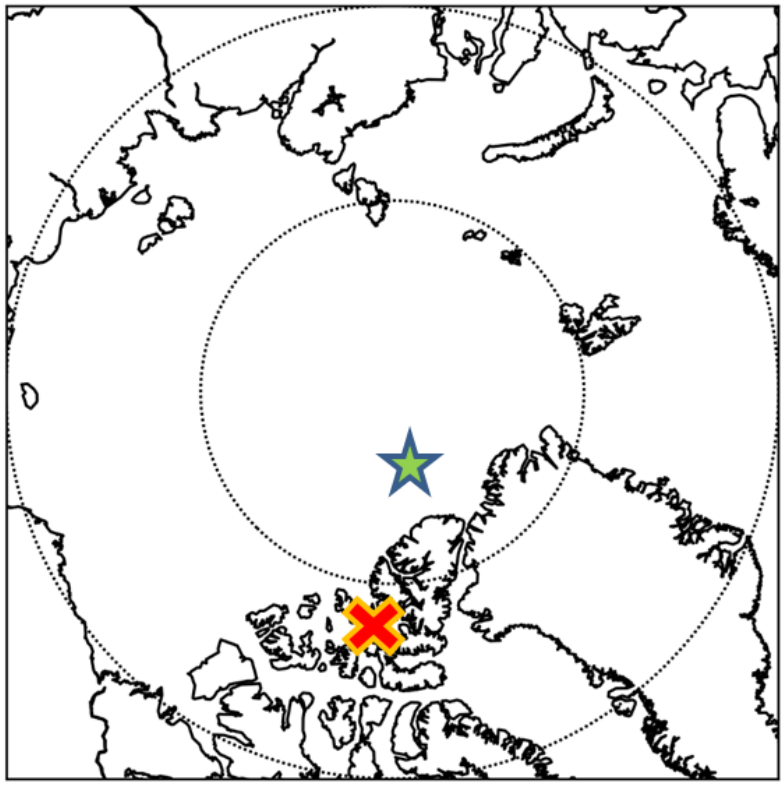

Figure 1. Map of Arctic centred on North Pole. Stars show centre of model grids used in this study: green is Northwest Alert (NW Alert) grid; orange is Axel grid. Grid sizes are approximately 440 km (N-S) x 72 km (E-W).

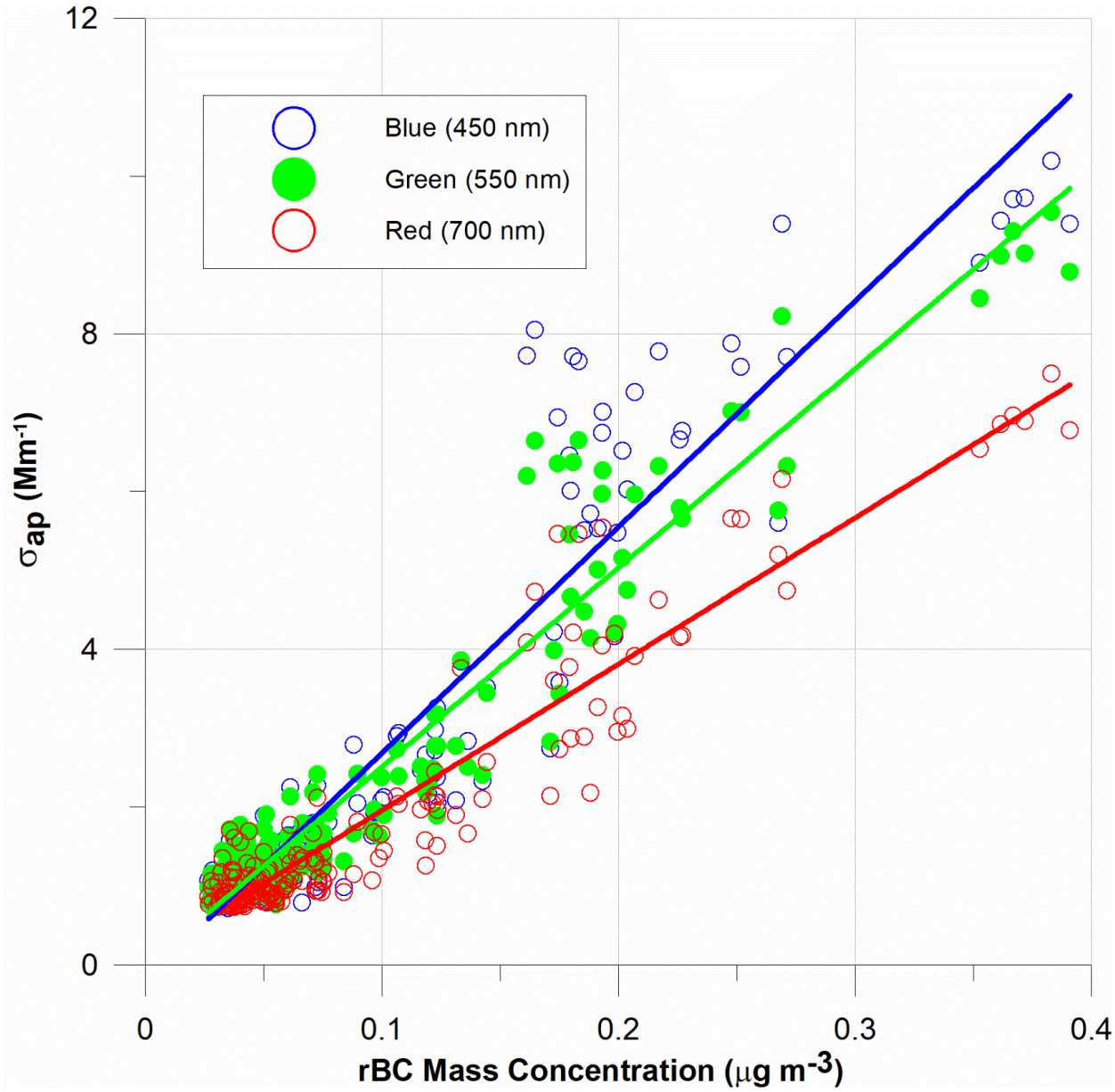


Figure 2. Particle light absorption coefficient ($\sigma_{ap}$) at three wavelengths (450 nm, 550 nm and 700 nm) plotted versus refractory black carbon (rBC) mass concentrations for all above-detection-limit data collected during POLAR 6 flights from Alert, Nunavut, Eureka, Nunavut and Inuvik, NWT. Regression lines shown for reference.

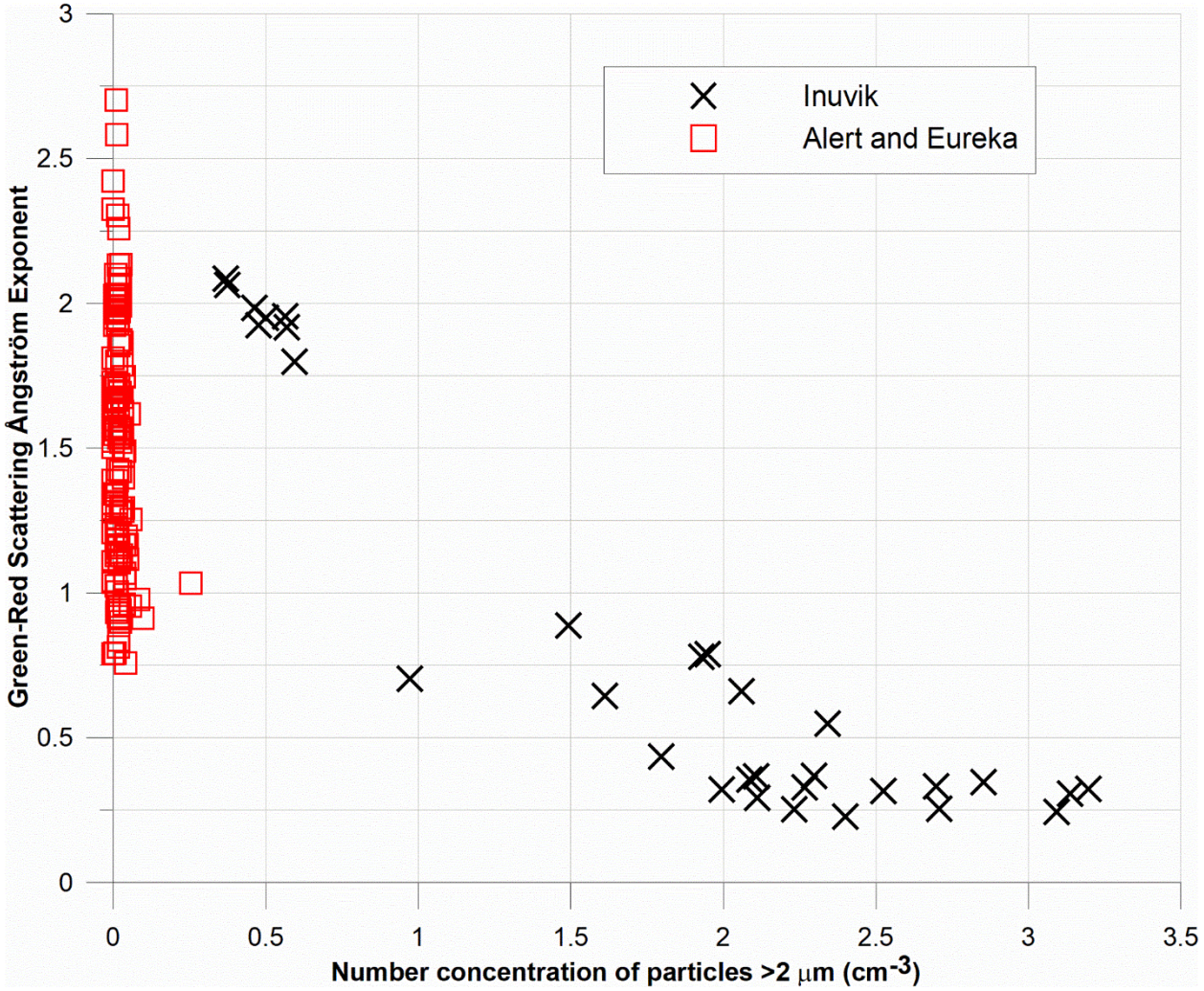


Figure 3. Light-scattering Angstrom exponent between green and red wavelengths plotted versus the number concentrations of coarse particles (> 2 μm diameter). Data are separated between those collected during flights from Alert and Eureka (red boxes) and from Inuvik (black crosses).

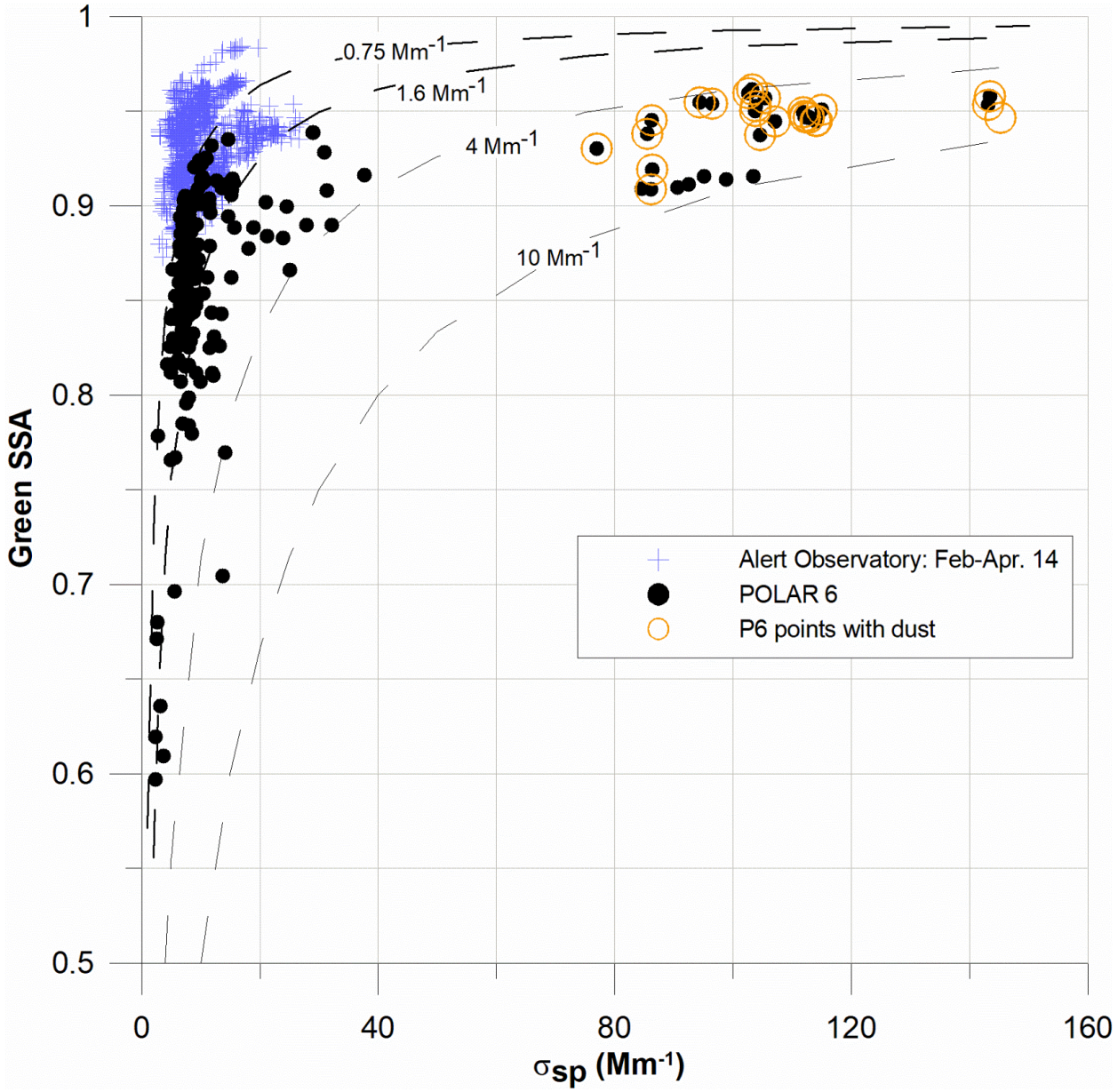


Figure 4. Single scattering albedo (SSA) at the green wavelength (550 nm) plotted versus the particle light scattering coefficient ($\sigma_{sp}$) at 550 nm. Data are separated between those collected at the Alert Observatory (blue crosses) and those collected from the POLAR 6 aircraft (black dots). In addition, points influenced most strongly by dust are circled in orange. Line of equal particle light absorption ($\sigma_{ap}$) are for reference.

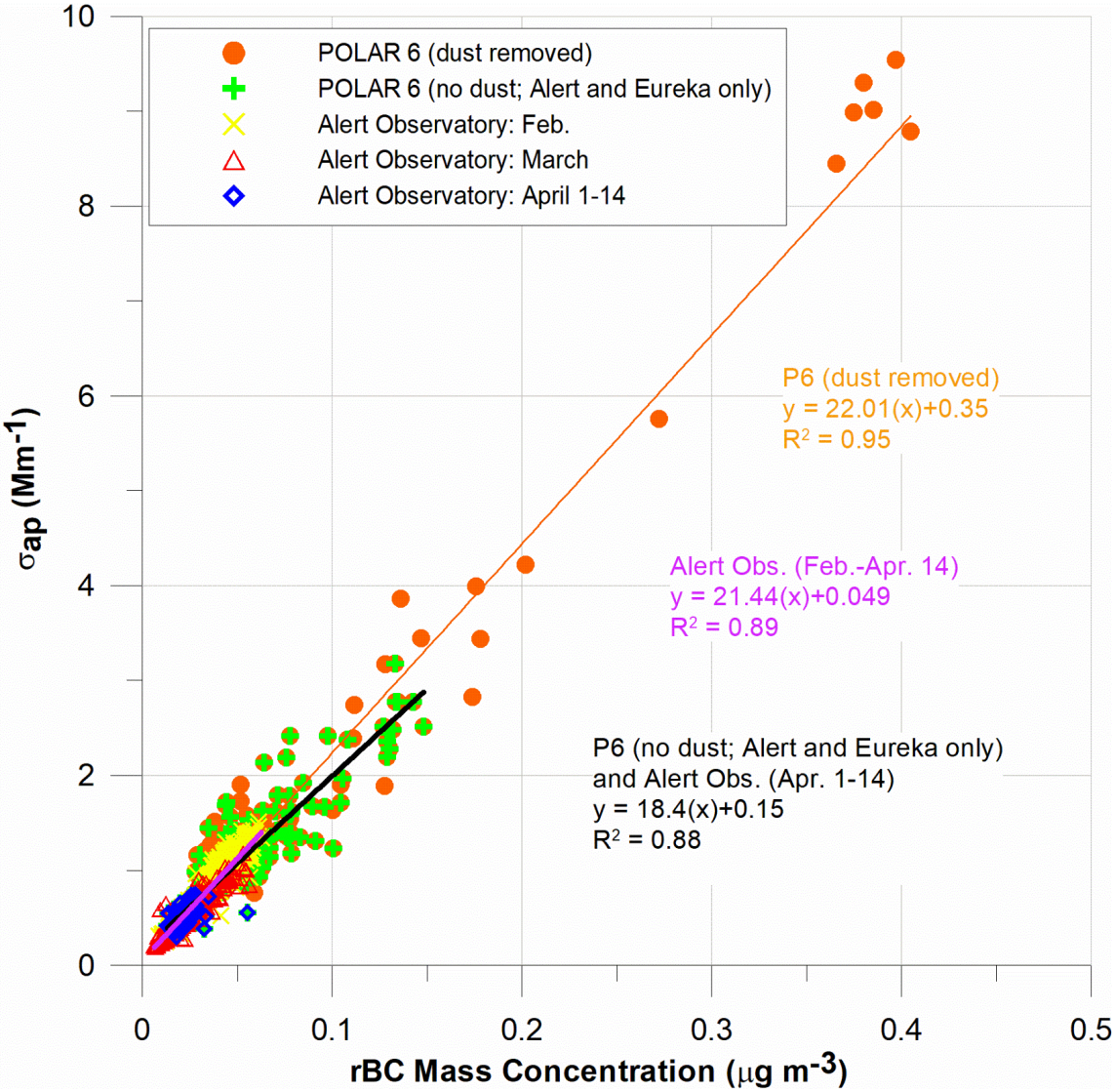


Figure 5. Particle light absorption coefficient ($\sigma_{ap}$) at 550 nm plotted versus refractory black carbon (rBC) mass concentrations for all above-detection-limit data collected during POLAR 6 flights from Alert, Eureka and Inuvik, NWT, with major dust influence removed (orange dots), for data collected during POLAR 6 flights from Alert and Eureka only (green crosses) and for data collected at the Alert Observatory. The Alert Observatory data are separated between those collected during February, during March and during April 1-14, where the latter corresponds mostly closely with the POLAR 6 flights out of Alert and Eureka. Regressions are shown for all POLAR 6 data (major dust removed; orange curve), for all Alert Observatory data (purple curve) and for the POLAR 6 data from Alert and Eureka combined with the Alert Observatory data for April 1-14 (black curve).

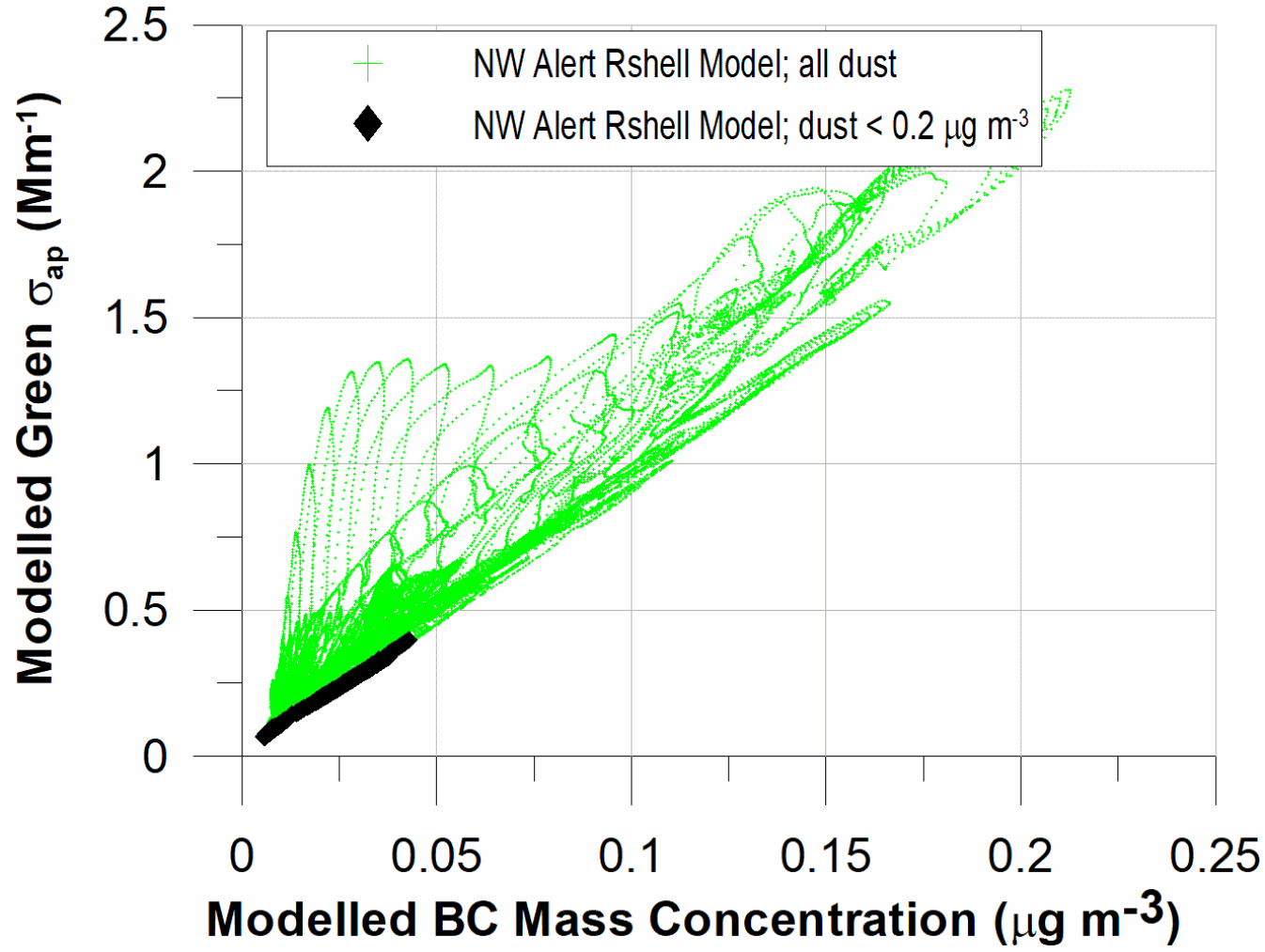


960 Figure 6. Modelled light absorption coefficients ($\sigma_{ap}$) at 550 nm plotted versus black carbon (BC) mass concentrations for the NW Alert grid and the 'Rshell' assumption (green). The black diamonds indicate the data limited to those points with dust concentrations less than 0.2 μg $m^{-3}$.

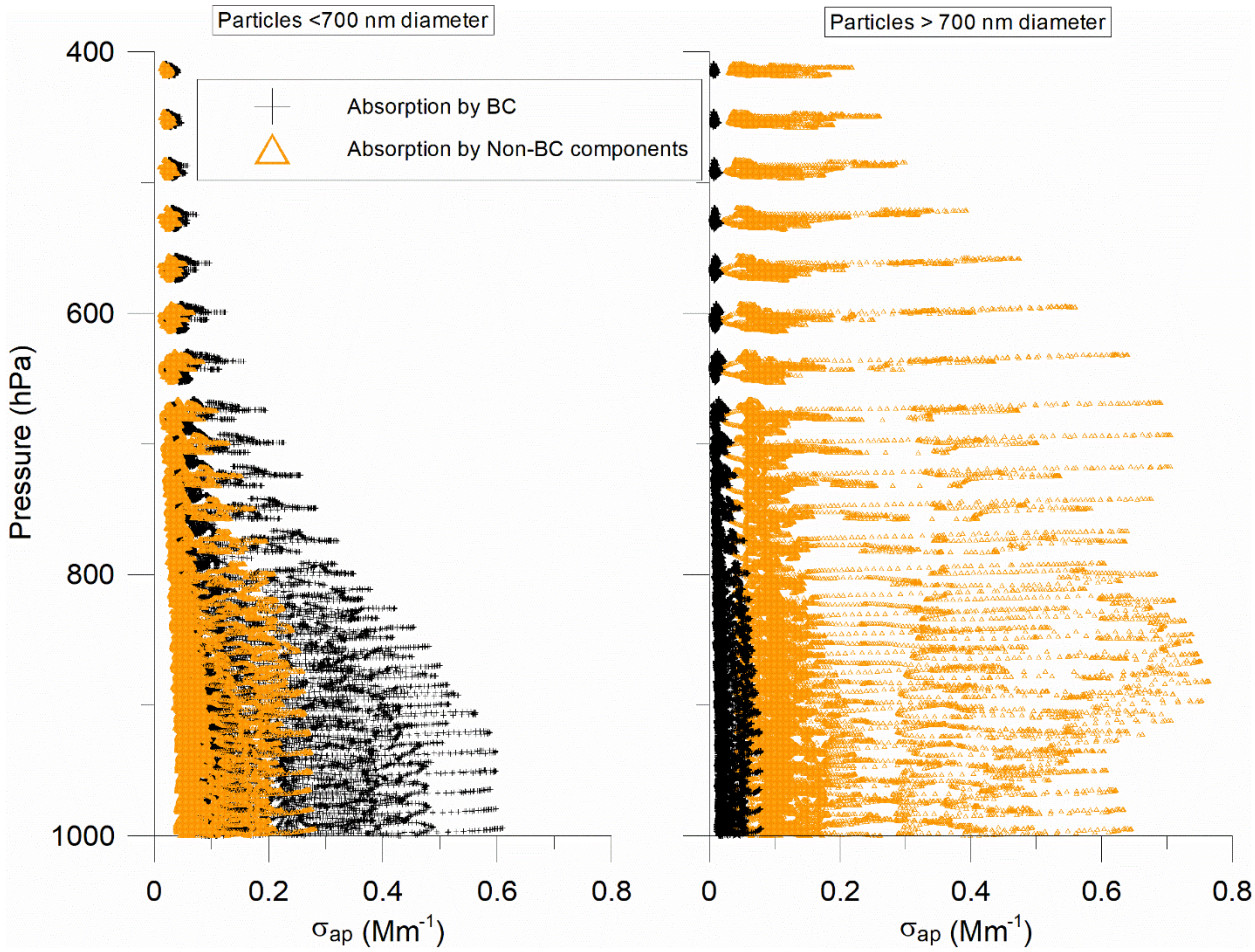


965

Figure 7. Modelled profile data of the contributions to absorption from BC (black crosses) and non-BC absorbing components (orange triangles) for a) particles less than 700 nm diameter and b) particles >700 nm diameter. The simulations are for the NW Alert grid box and based on an external mixture.

970

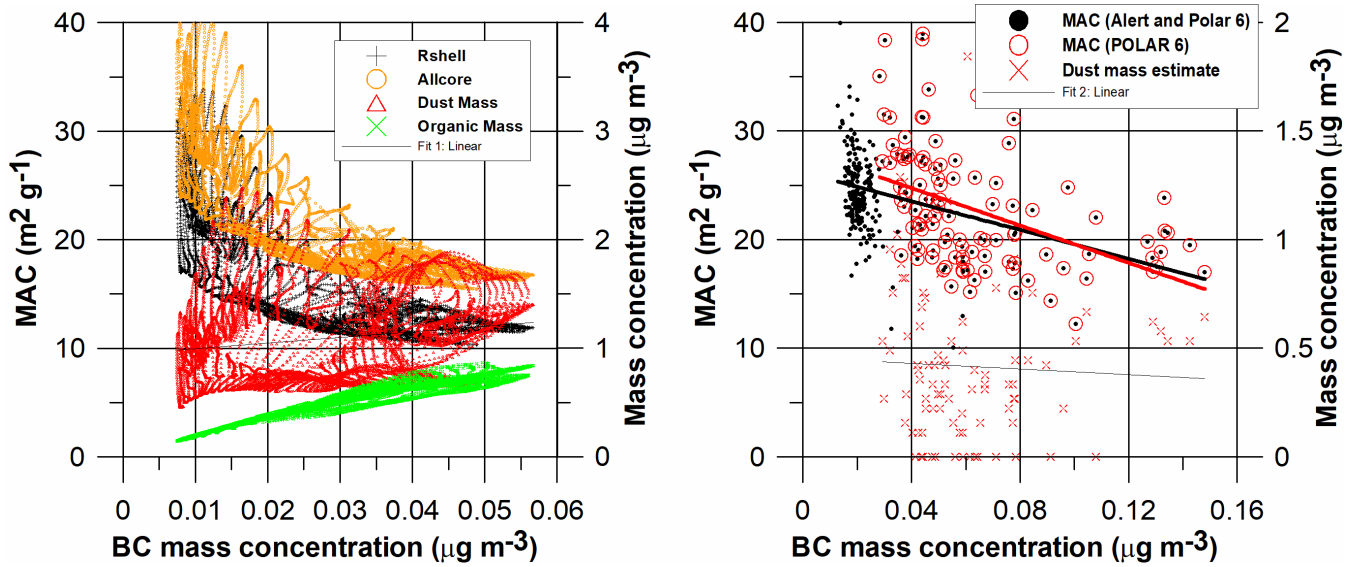


Figure 8. a) Modelled BC Mass Absorption Coefficient (MAC) plotted against modelled BC for the 'Allcore' (orange circles) and the 'Rshell" (black crosses) assumptions; modelled dust mass concentrations constrained to dust less than 1.5 μg $m^{-3}$ versus modelled BC mass concentrations (red triangles); modelled organic aerosol (OA) mass concentrations versus BC mass concentrations (green crosses); all modelled values are for April 1-14, 2015. b) MAC values from POLAR 6 flights and Alert Observatory (April 1-14) plotted versus measured refractory black carbon (rBC) mass concentrations (black dots); dust mass concentrations (red crosses), estimated from particle size distributions onboard the POLAR 6, plotted versus rBC mass concentrations; MAC values associated with POLAR 6 measurements only identified (red circles). The confidence level in the negative slope of the black points is greater than 99%.

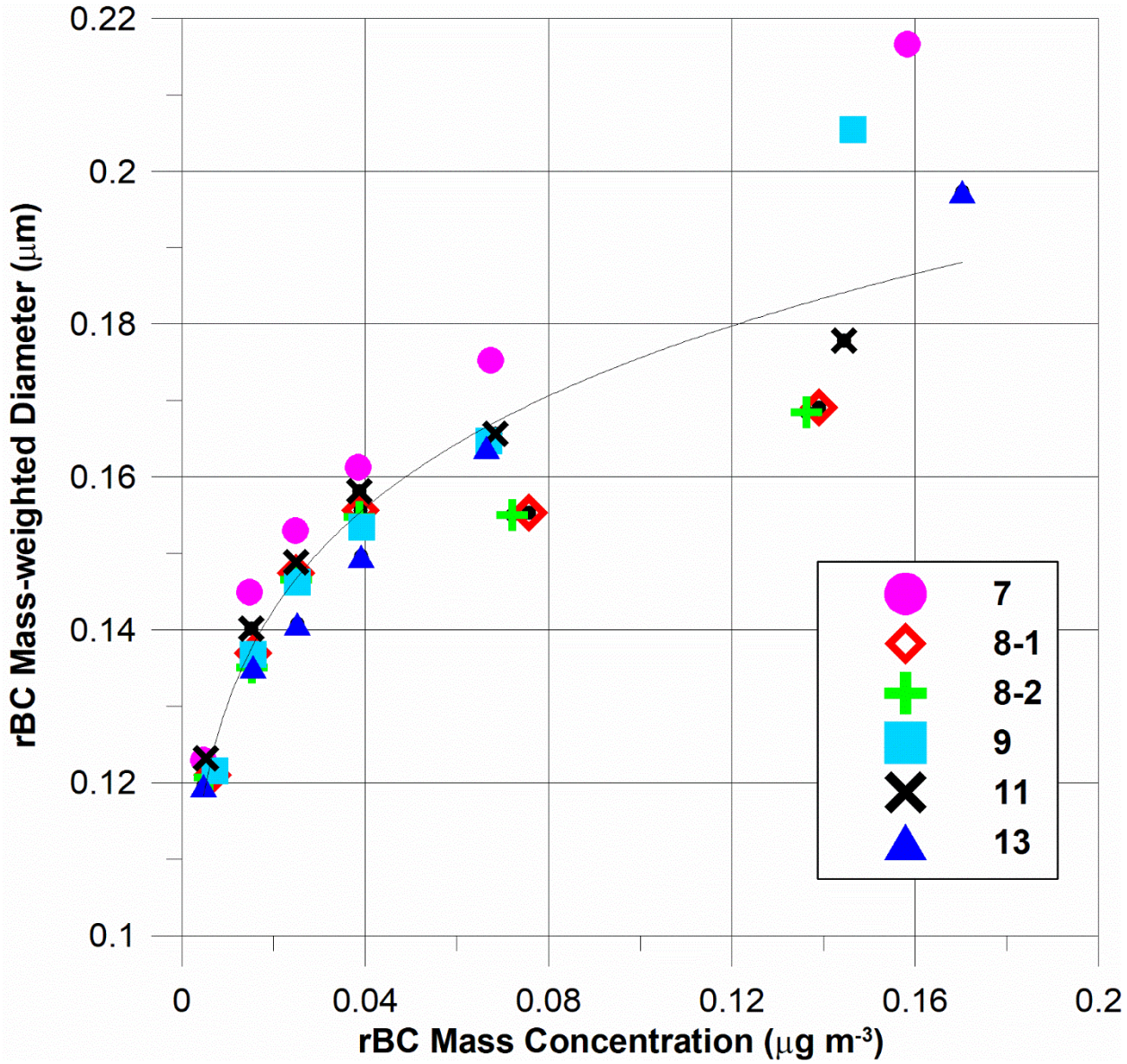


Figure 9. Mean mass-weighted diameters of rBC measurements versus rBC mass concentrations, assuming spherical rBC components. Points are averages for mass concentration intervals of 0-0.01, 0.01-0.02, 0.02-0.03, 0.03-0.05, 0.05-0.1 and 0.1 to the maximum observed. The power-law fit ($y=0.237[x^{0.129}]$) is through all points with an $R^2$ of 0.89 and confidence level of better than 99%. The power law is appropriate based on the relationship between diameter and mass of a sphere, which includes the diameter going to zero as the mass goes to zero.

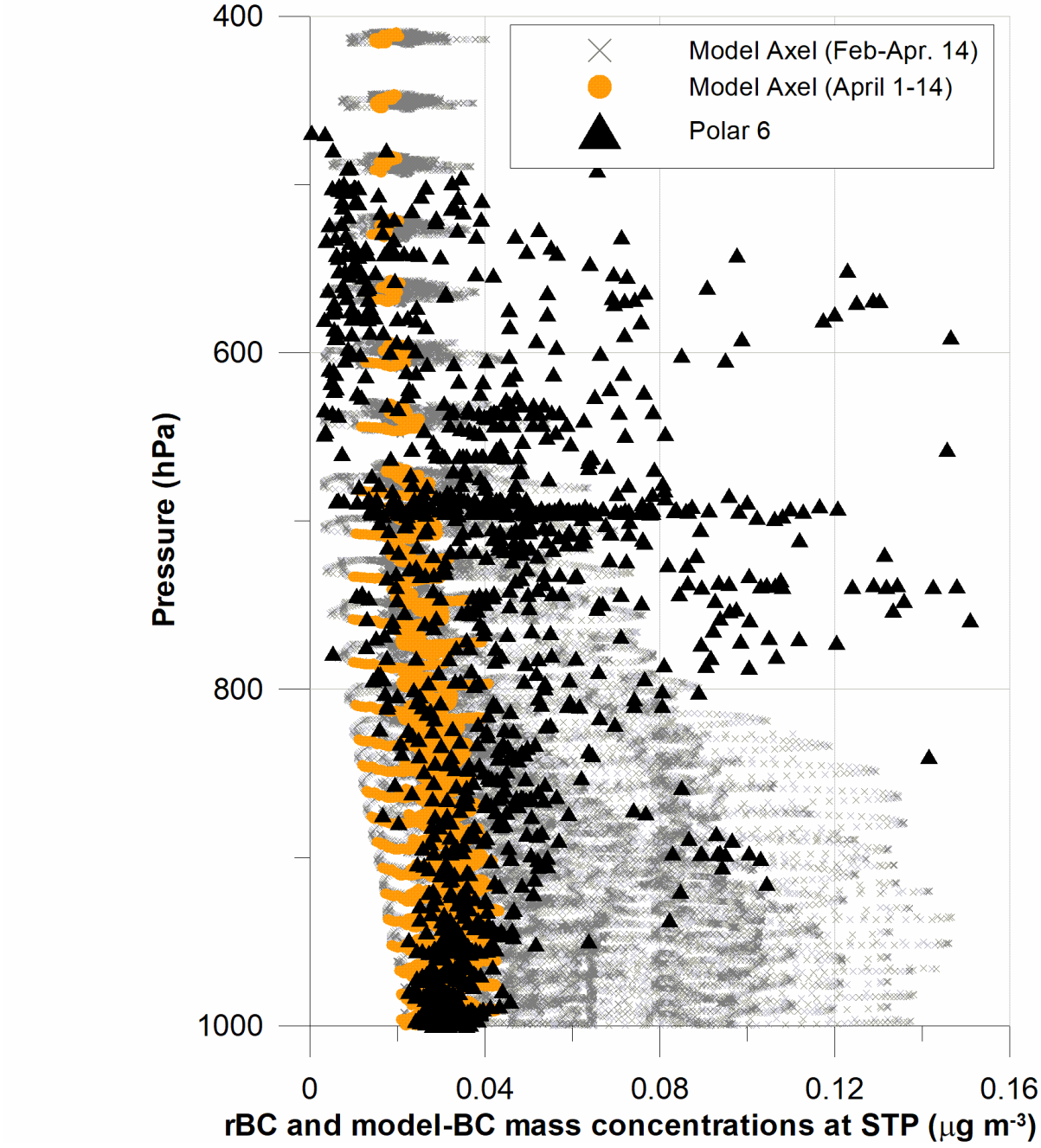


Figure 10. Vertical profile plot of BC mass concentrations from the model for the Axel grid (green crosses for Feb.-Apr. 14, inclusive; red crosses for April 1-14 only) and rBC mass concentrations from the POLAR 6 observations plotted with pressure.

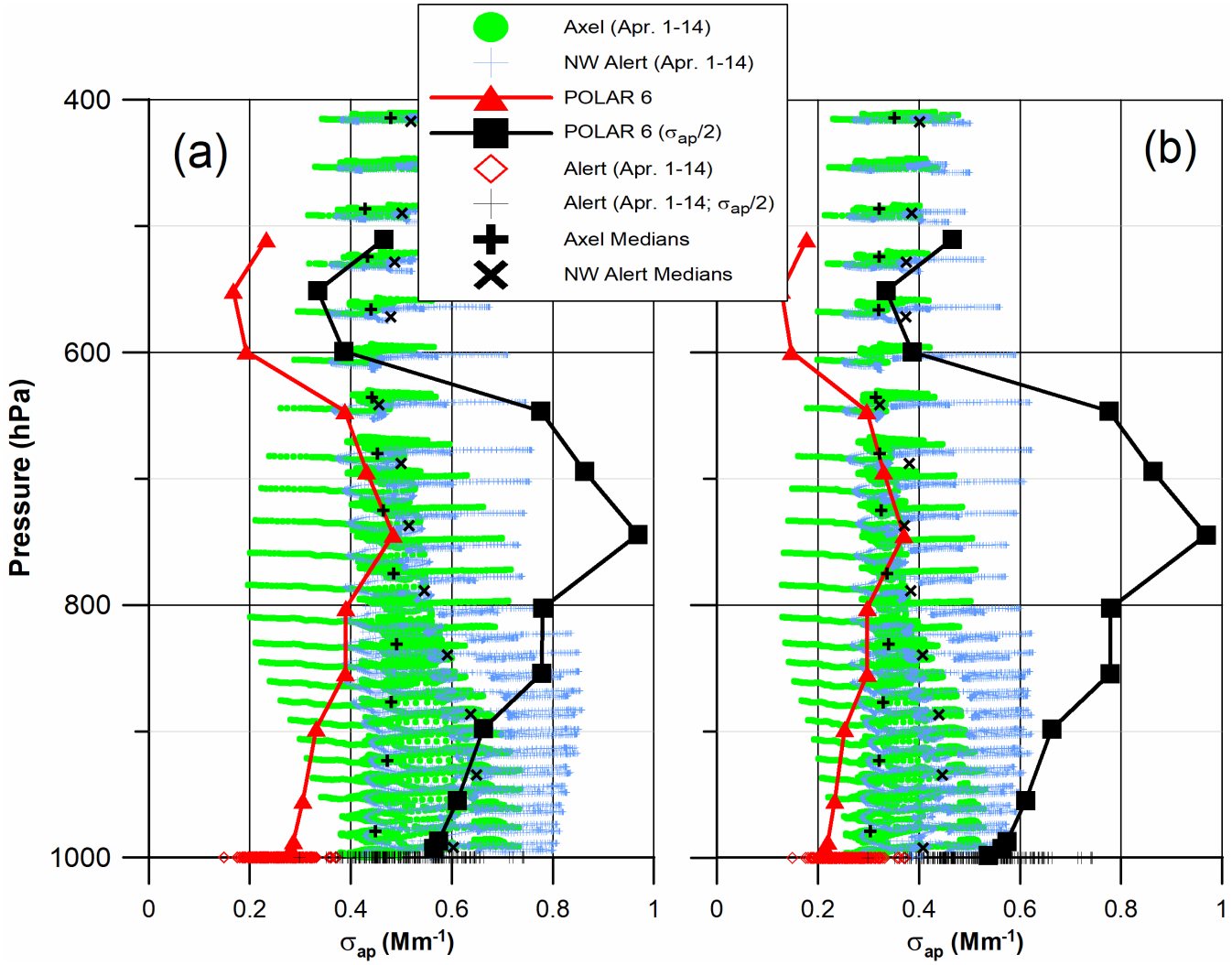


Figure 11. Vertical profile plots of $\sigma_{ap}$ with atmospheric pressure showing median values based on POLAR 6 observations (black points). Red points represent the POLAR 6 $\sigma_{ap}/2$. Data from the Alert Observatory for April 1-14 are shown for $\sigma_{ap}$ (black squares) and $\sigma_{ap}/2$ (red squares). The model results are for April 1-14 with the green dots representing the Axel grid and blue crosses representing the NW Alert grid: (a) model results for the 'Allcore' assumption; (b) model results for the 'Rshell' assumption.

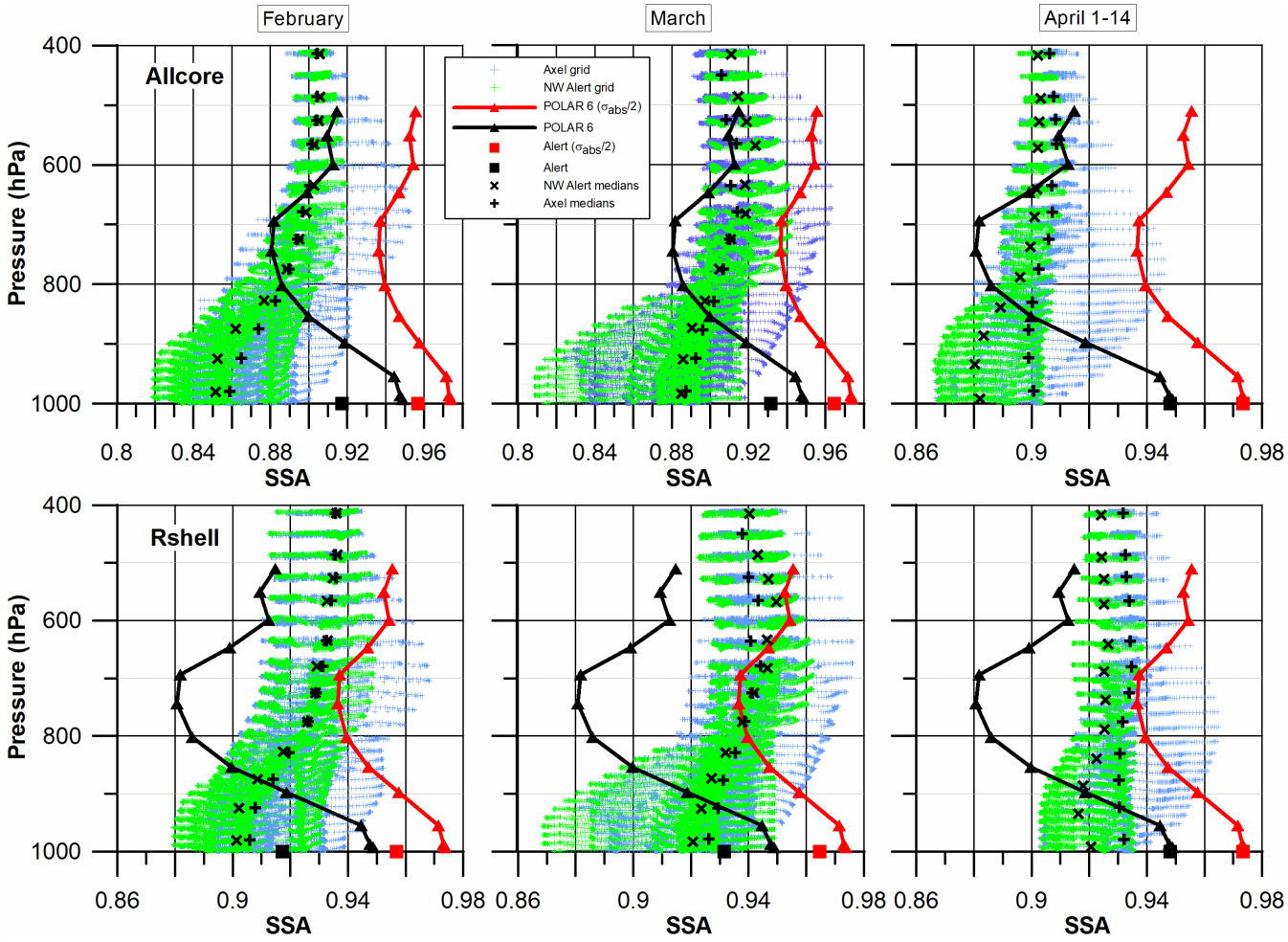


Figure 12. Vertical profile plot of SSA with atmospheric pressure showing modelled results for February (a), March (b) and April 1-14 (c) based on the 'Allcore' assumption and results for February (d), March (e) and April 1-14 (f) based on the 'Rshell' assumption. Median values of SSA from the POLAR 6 observations and the Alert Observatory shown in a, b and c are based on the measured absorption (black points) and the assumption of $\sigma_{ap}/2$ (red points).

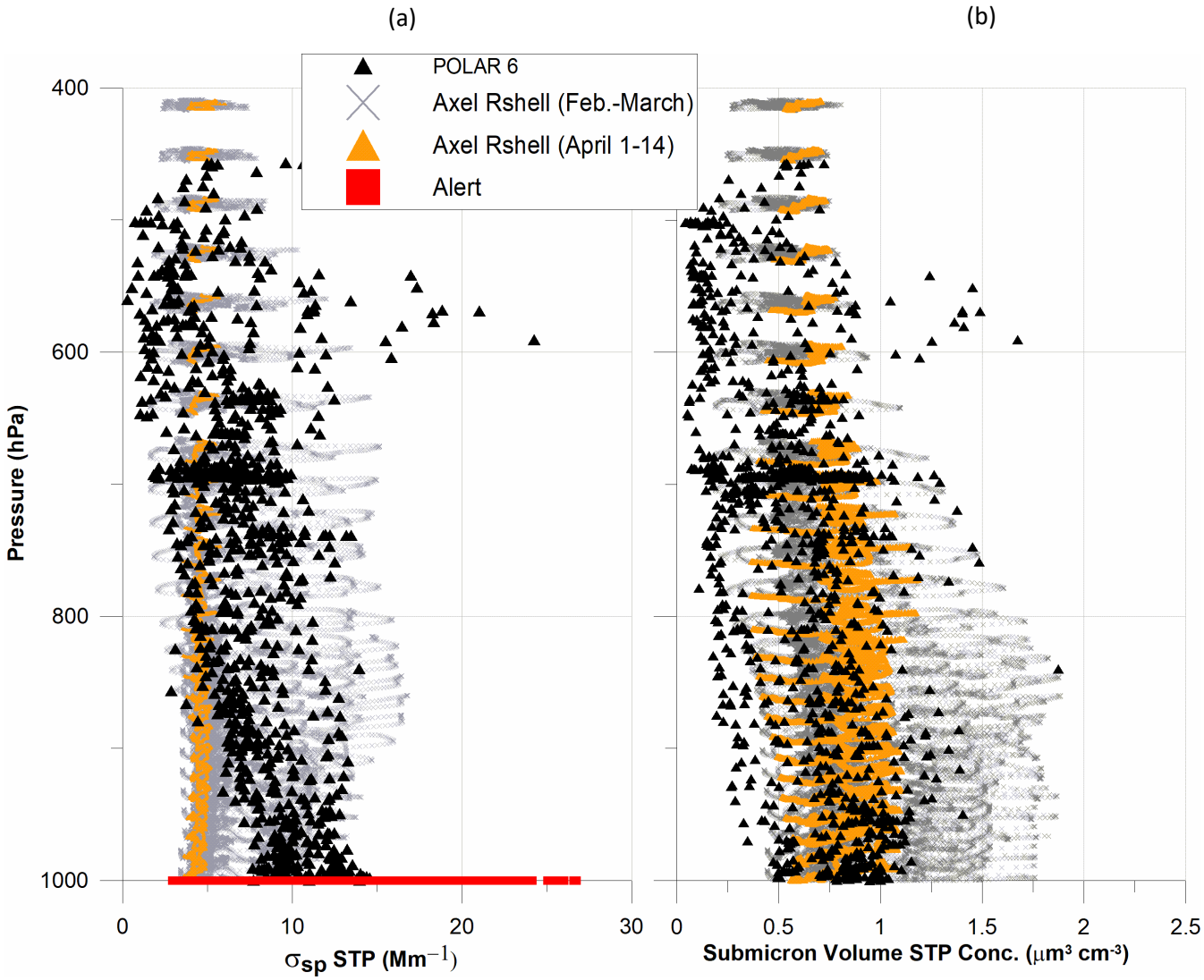


Figure 13. a) Vertical profile plot of $\sigma_{sp}$ from the model for the Axel grid (green crosses for Feb.-Apr. 14, inclusive; red crosses for April 1-14 only) and $\sigma_{sp}$ from the POLAR 6 observations plotted with pressure. Also shown are the Alert Observatory $\sigma_{sp}$ for April 1-14. b) As in a), but for submicron volume concentrations from the model simulations and POLAR 6 observations. Volume concentrations from the Alert Observatory are not shown.

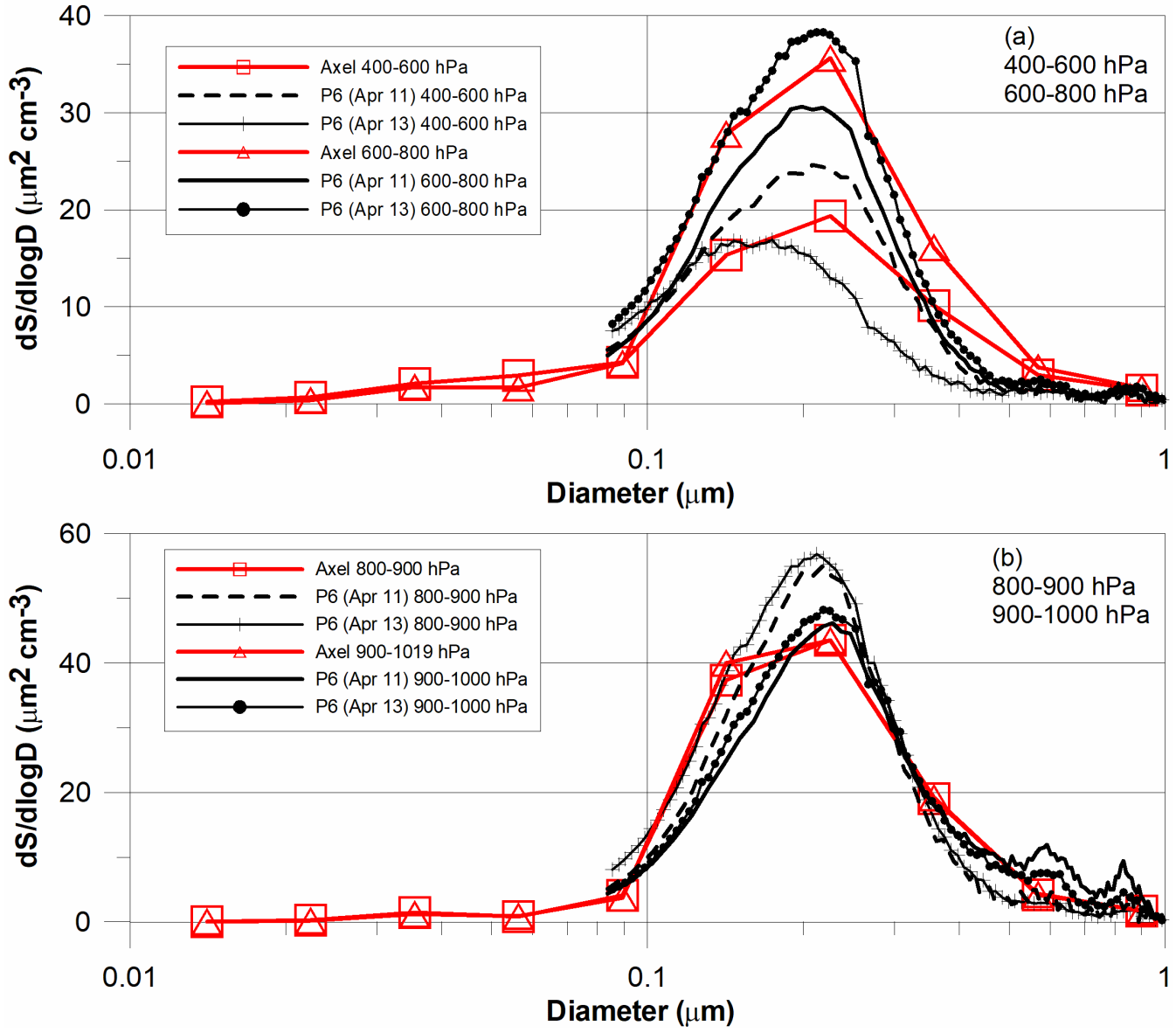


Figure 14. Comparison of modelled size distributions for the Axel grid and period of April 1-14 with the measured distributions from the POLAR 6 (P6) flights on April 11 and 13. All distributions are averaged for the indicated pressure intervals. a) Modelled and measured distributions for pressure intervals of 400-600 hPa and 600-800 hPa. b) Modelled and measured distributions for pressure intervals of 800-900 hPa and 900-1000 hPa.

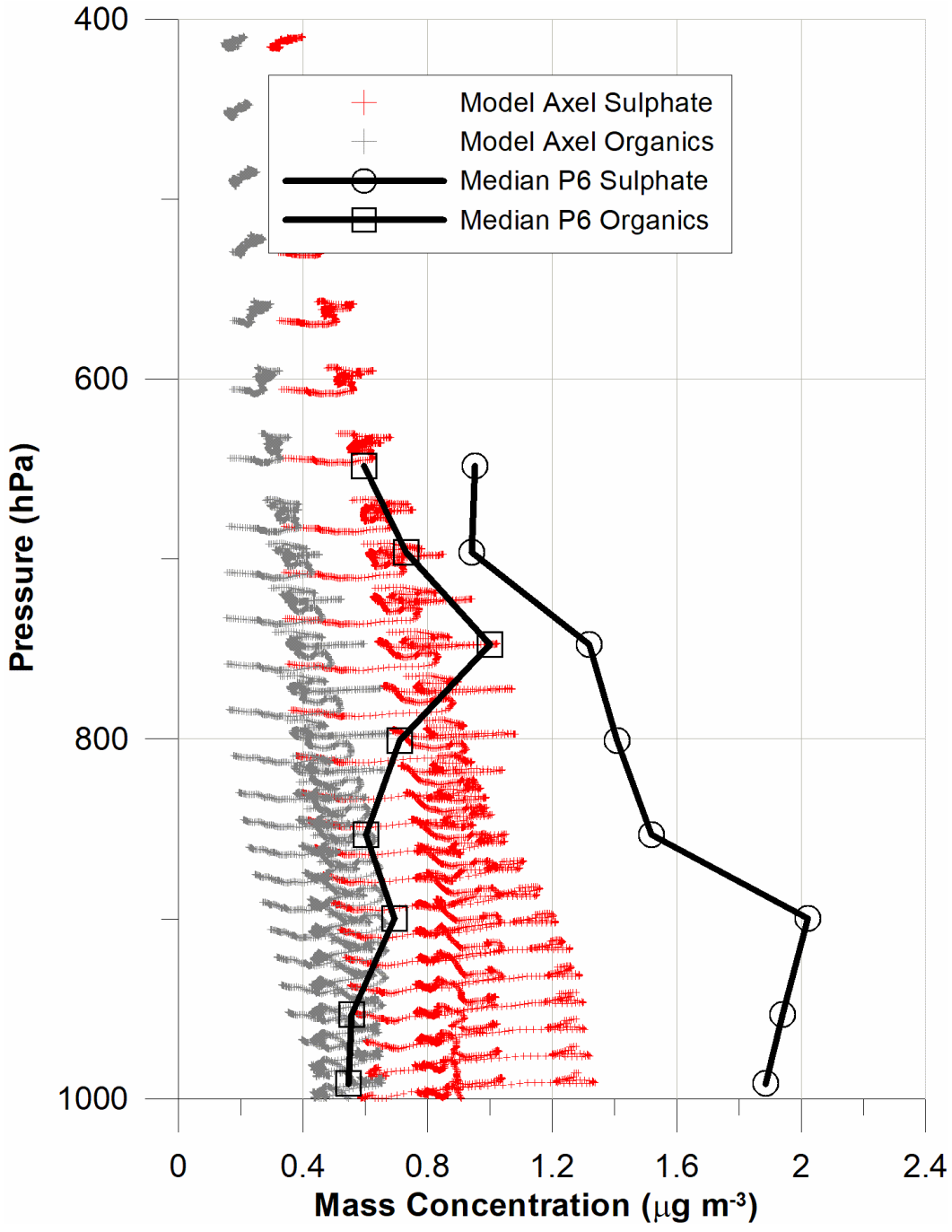


Figure 15. Vertical profile plot of mass concentrations of sulphate and of organics with pressure from the model for the Axel grid for April 1-14 (red crosses are sulphate and green crosses are organics) and median values of the POLAR 6 sulphate (open circles) and organic (open squares) mass concentrations.